AN INVESTIGATION ON WHETHER OR NOT OUR UNIVERSE IS FRIEDMANNIAN ON LARGE SCALES

BY

WAMALWA DISMAS SIMIYU

MSC/0014/99

A Thesis submitted in partial fulfilment for the degree of

MASTER OF SCIENCE

IN

THEORETICAL PHYSICS

MASENO UNIVERSITY

SEPTEMBER 2002

ABSTRACT

According to the cosmological model that has been widely accepted for a long time, our universe at large is well described by a Friedmann model in which the universe has been expanding from a short time after a very hot, almost point-like "big bang". The Friedmann universe embodies the cosmological principle according to which our universe, at large scales, should look homogeneous and isotropic. Nevertheless, as galaxy redshift surveys based on distance measurements probe deeper into the universe, they uncover larger and larger structures, such as sheets, clusters and superclusters, walls and voids that give evidence of inhomogeneity at all scales, hence point to a fractal universe. This raises the question as to whether, at some scale, our universe can indeed be modeled by the Friedmann universe. This question together with the Einstein's equations of dynamics and evolution of the universe based on the Friedmann metric are introduced in chapter 1. In chapter 2, the problem posed by catalogues that involve distance measurements and hence point to fractality has been made much clearer by discussing various methods used to obtain these distances. Misinterpretations of observational data obtained through such distance measurements is also discussed. In chapter 3, a method that does not rely on distance measurements but on redshift, light intensity and number density of galaxies has been clearly explained and the relevant Einstein's equations derived. The analytic and graphical evaluation of the results(computer simulations) for the functional inter-dependence of the above astronomical quantities are obtained in chapter 4. Finally, the work is concluded and recommendations made in chapter 5.

CHAPTER ONE

1. INTRODUCTION

Questions about the universe, for instance concerning the formation of galaxies and large-scale structures, have puzzled man for a very long time. This has led to a lot of research [1,2,3,4,5,6,7-9] work in this area. The branch of Physics that addresses such questions is Cosmology. The basis of Cosmology nowadays is Einstein's theory of General Relativity. According to this theory, space-time is not flat like in Special Relativity but curved in such a way that the worldlines of bodies freely falling in a gravitational field are the geodesics of the space-time metric [10]. Einstein formulated this theory in 1915. The metric is related to the matter distribution in space-time by the general Einstein's equation:

$$G^{\mu\nu} = BT^{\mu\nu} \tag{1}$$

where $G^{\mu\nu}$ is the Einstein tensor related to the Riemann curvature of the space-time metric, $g_{\mu\nu}$; $T^{\mu\nu}$ is the stress-energy tensor describing the energy-momentum densities and currents associated with non-gravitational matter and fields, and B is given in terms of the gravitational constant G and speed of light c as $B = 8\pi G c^{-4}$; and the indices μ, ν run from 0 to 3. On a very large scale, the universe consists of clusters of galaxies. Several clusters of galaxies can be seen in the largest telescopes. From a cosmological point of view, galaxies are the 'atoms' of the universe, and their distribution, motion, and origin need to be explained [11]. For a long time the distribution of these galaxies in the universe was believed to be homogeneous and isotropic on large scale. The experimental evidence for this belief was taken from [12]:

1. The distribution of galaxies in the sky.

2. The linearity of the redshift-distance relation (Hubble law).

3. The isotropic distribution of the radio sources in the sky.

4. The isotropy of the cosmic micro-wave background radiation (CMBR).

These facts, together with the cosmological principle which says that the universe is homogeneous and isotropic, have faced challenges in recent years. This is because Theoretical Cosmology employs physical laws established on the earth, and makes the daring extrapolation that they apply throughout the universe. This extrapolation is not enough [11] because the situation about the universe may not look the same for observers not located on the earth. To escape from the prison of the single vantage point, there was therefore need for something more: a cosmological principle. The principle is essentially philosophical in nature, and seems to complement the laws of physics rather than follow from them. It basically says that we are not in any preferred position. However, in recent years, big catalogues have been compiled that list objects in the sky and give their distance from us as well as the direction from which their light reaches us. So we obtain a three-dimensional picture of the luminous matter in the universe. While the two-dimensional projection that we see by looking at the sky seems to be fairly isotropic, the three-dimensional distribution seems to show inhomogeneity at all scales. This is philosophically disturbing: the most natural and naive expectation, confirmed by the isotropy of the two-dimensional projection, was to assume that the universe looks isotropic to us. Then the cosmological principle says that it must look the same to every observer in the universe (at rest with respect to the background). But isotropy at every point in an analytic universe implies homogeneity. So the observations showing that the three-dimensional distribution of galaxies seem to show inhomogeneities at all scales came as a big surprise.

One important problem is how to distinguish between 'small' and 'large' scale structures. Obviously, at smaller scales than galactic scales, things look very inhomogeneous. But how could one tell in practice if, from a given scale onwards, the universe starts to look homogeneous and isotropic? To discuss this, we could assume, for instance, that the universe is fractal rather than homogeneous at large scale. By fractal we mean a system in which more and more structures appear at larger and larger scales and the structures at small scales are similar to the ones at larger scales [13]. Evidence of fractality like the existence of voids and walls comes from the three-dimensional catalogues. Starting from a point occupied by an object, we count how many points are within a volume characterized by a certain "length" relation from which one can define the fractal dimension. A relation between N ("mass") and r ("length") is defined as:

$$N(r) = Ar^F$$

where F is the fractal dimension and A is the lower scale , r_0, up to which the self-similarity holds and it is also related to the elementary objects N_0 that are present within r_0 by

$$A = \frac{N_0}{{r_0}^F} .$$

It is further argued that fractals are irregular systems at all scales and the self-similarity that characterizes their properties implies the absence of regularity or analyticity everywhere in the system. In an analytic universe, isotropy automatically implies homogeneity. This is not the case in a non-analytic or fractal universe.

According to the current picture of the universe, most of the mass is contained in a dark component formed by collisionless dust-like particles without pressure, interacting only via Newtonian gravity [14]. The observed large-scale structures are generated by the

evolution of initially minute density fluctuations. The initial density fluctuations trigger gravitational instabilities, hence the initially uniform background condensates into large-scale structures. However, it has been a long-standing matter of debate as to whether the gravitational instability is able to produce so much inhomogeneity in the time provided by the age of the universe.

Since we cannot perform experiments on our universe, there is need to come up with an idealized model of our universe and then compare the predicted observations in that model with the observations performed in our universe. One such model is the Friedmann model. In this model, the cosmological principle is implemented as follows: there is a preferred time coordinate t such that the t=constant slices are homogeneous and isotropic spaces. There are basically three simply connected isotropic and homogeneous spaces: the sphere (constant positive curvature), flat space (no curvature), and hyperbolic space (constant negative curvature). By means of stereographic projection, the three cases can be handled in a uniform manner. The metric of the Friedmann universe then reads:

$$g = c^2dt^2 - \frac{R^2(t)}{(1+\kappa r^2)^2}\,(dx^2 + dy^2 + dz^2)$$

where $r^2 = x^2 + y^2 + z^2$ (in a rectangular coordinate system on the three-dimensional projection space); $\kappa = 1, 0, -1$ for the spherical, flat, hyperbolic cases, respectively; $R(t)$ is the cosmic scale factor (that is, the radius of the universe at time t for the case of the unit sphere, $\kappa = 1$); c is the speed of light. In spherical coordinates on the projection space, the metric reads:

$$g = c^2dt^2 - \frac{R^2(t)}{(1+\kappa r^2)^2}\,(dr^2 + r^2d\theta^2 + r^2sin^2\theta\, d\varphi^2)\,.$$

In order to make predictions about the dynamic evolution of our universe based on

the Friedmann model, one proceeds to solve the Einstein's field equations which, for this metric, reduce to the following two equations:

$$12\kappa c^2 + 3R'^2(t) = Bc^4 R^2(t)\rho(t) \tag{2}$$

and

$$4\kappa^2 c^2 + 2R(t)R''(t) + R'^2(t) = -Bc^2 R^2(t)p(t), \tag{3}$$

where

$$R'(t) = \frac{dR}{dt}\ ; \quad R''(t) = \frac{d^2R}{dt^2};$$

$\rho(t)$ is the mass density of matter in the universe at time t and $p(t)$ is the pressure of matter in the universe at time t. Furthermore, Einstein's field equations are supplemented by an equation of state relating $p(t)$ and $\rho(t)$. Particularly relevant are two cases:

1. $\rho(t)\ R^4(t)$=constant (for radiation-dominated universe, $p(t) = \frac{1}{3}\ \rho(t)$)
2. $\rho(t)\ R^3(t)$=constant (for matter-dominated universe, $p(t) = 0$).

Researchers in this field claim that the distribution of visible matter is not uniform on any scale but rather fractal. Since we believe today that our universe is matter-dominated, this raises the question as to whether or not our universe can be modeled by the Friedmann universe. The answer probably depends on how much dark matter there is and how it is distributed in the universe. The idea of fractality comes from three-dimensional maps of the universe. These maps depend on our ability to measure distance. The distance measurements involve a complicated ladder of measurements proceeding from small distances to ever larger distances. At each rung of this ladder, some physical assumptions have to be made. In more or less hidden form, the assumption that the universe is Friedmann may enter into these measurements. Yet these same catalogues seem to raise the question as to

whether the universe is indeed Friedmann. So, methodologically, it would be clearer to try to address that latter question using direct observations which do not involve assumptions about the space-time.

1.1 STATEMENT OF THE PROBLEM

To investigate from data that does not involve distance measurements, if it is possible to rule out that luminous matter is homogeneously distributed in accordance with the Friedmann universe.

1.2 SIGNIFICANCE OF THE STUDY

The assumption that the universe at large is well modeled by a Friedmann universe has become so much part of physicists' world view, that the idea of giving it up would appear revolutionary to the majority of scientists. According to this model which embraces the cosmological principle, matter in the form of neutrons and protons was very hot and dense prior to about one second after the 'big bang '. As the universe expanded, the temperature fell and some of these nucleons were synthesized into light elements: deuterium and helium. Theoretical calculations for the nuclear processes predict, for instance, that about a quarter of the universe consists of helium which is in agreement with current stellar observations. About ten thousand years later after the 'big bang', the temperature had fallen to such an extent that the energy density of the universe began to be dominated by massive particles of which we are partly made, rather than the light and other radiations which had predominated earlier. So it is very important to solidly establish whether experimental evidence forces us to abandon the Friedmann model or not.

1.3 AIM AND OBJECTIVE OF THE STUDY

To investigate whether or not luminous matter is homogeneously distributed in accordance with the Friedmann universe.

CHAPTER TWO

2. LITERATURE REVIEW

For a long time our universe has been known to be homogeneous and isotropic on the largest length scales. This type of universe is well described by the Friedmann model. The Friedmann model embodies the cosmological principle. According to this principle, that has been widely accepted for a long time, our universe at large is well described by a Friedmann model in which the universe has been expanding about every point in space from a short time after a very hot, almost point-like 'big bang'. The violent explosion resulted in particles rushing away from each other in a super-dense phase. The fact that galaxies are receding from us is a consequence of this initial explosion and was first discovered observationally by Hubble [15] between 1923 and 1929. Projecting galaxy trajectories backwards in time means that they converge to a high density state i.e., the initial fireball.

In 1964, Penzias and Wilson [4] discovered an isotropic radio background which was a relic left-over from the primordial fireball. This micro-wave background radiation was considered as the isotropy of the universe and is in line with the theoretical predictions of a Friedmann universe.

In 1986, de Lapparent, Geller, and Huchra demonstrated [9] the existence of filaments and sheets from scales of 25Mpc to over 100Mpc. Their surveys also showed that radio galaxy and quasar surveys indicate homogeneity on scales of over 100Mpc i.e., nearly a billion light years. In April 1992, COBE satellite team announced the discovery of anisotropies in the cosmic micro-wave background radiation at the level of one part in 100,000. This map of the sky is considered as the best evidence for the isotropy or spherical symmetry of the universe.

In 1995-96 Hubble Space Telescope improved the determination of Hubble's constant which relates the velocity and distance of a receding galaxy from us. Progress in understanding our universe has been strongly linked to the development of telescopes and detectors. The availability of data from large telescopes on earth enabled Hubble [15] to do substantial work in surveying the universe. He established an extragalactic distance scale, the expansion of the universe, and apart from noting evidence of large-scale homogeneity and isotropy of the universe, he also detected clustering of galaxies, which pointed to existence of inhomogeneities. From the above discussion, it seems clear that the observations made on our universe reveal a homogeneous and isotropic large scale picture of it. However, further work [16,17,18,19,20] done on the statistical analysis of the immense observational data we have for the universe give a different picture from the one above. Today, on the one hand, there are 4-metre class telescopes with very sensitive detectors. On the other hand, modern satellites have given us much direct evidence about our universe. The observational data obtained from them has posed a challenge to the old existing ideas about our universe including the cosmological principle. Most researchers now claim that the distribution of visible matter is not uniform on any scale but rather fractal all through. Therefore, they claim that fractals are irregular systems at all scales. By fractal we mean a system in which more and more structures appear at larger and larger scales and the structures at small scales are similar to the ones at large scales [13]. The existence of structures like galaxies in clusters and voids is believed to point towards inhomogeneity and therefore, raises the question as to whether or not the matter distribution really becomes homogeneous at a certain scale.

Among researchers in this field who claim that matter is fractally distributed are Labini

et al., [12] who explain the relation between homogeneity and Hubble's law by considering the redshift-distance relation. They note that, from observational data, there is a linear redshift-distance relation which, surprisingly, extends into the fractal structure. Since the fractal structure of matter is inhomogeneous at all scales, this seems to imply that there must be something besides the visible galaxies, which is uniformly distributed in the universe. This could be a homogeneous layer of dark matter. If the universe contained some substantial mass in the form of unknown dark matter, then only at scales where the homogeneous dark matter density dominates over the luminous inhomogeneous matter would the linear Hubble law apply. However, the explanation seemed to contradict the available data of classical Cosmology. It was then conjectured [12] that the Hubble law is a consequence of isotropy rather than of homogeneity, since in a fractal universe isotropy does not imply homogeneity. To save the linearity of the redshift-distance relation, it was suggested [12] that our galaxy is in a large void. This means that we are in a privileged position, while a typical place of a galaxy, belonging to the fractal structure, is within a fractal cluster [21]. This leaves the observed linear relation of the Hubble law as a mere accidental or luckily observed phenomenon of the universe due to our special position in it. It is therefore very clear that the argument presented here has several weaknesses and leaves a lot of questions to be asked about the fractal model of our universe.

Additional work in this area has been done by Pietronero et al., [22]. They address the problem of how to deduce meaningful galaxy correlations from observational data and discuss the various methods which have been used. The focus is on the volume limited three-dimensional samples and a new way is discussed to increase the scale of their statistical validity. From the available catalogues, it is argued [22] that the galaxy correlation

shows fractal properties with dimensions $F \approx 2$ up to the present observational limits ($200 - 800h^{-1}Mpc$ depending on the catalogue) without any tendency to homogenization. The first galaxy catalogues were only angular since they defined two angles corresponding to the galaxy positions in the sky [23]. These angular distributions show a small-scale structure, but appear smooth at larger angular scales. This situation was highly compatible with the expectation of a homogeneous universe according to theoretical predictions based on the Friedmann model. In the late nineteen seventies, when the first redshift measurement became available, it became possible to obtain the complete three-dimensional distribution of galaxies. Surprisingly, this distribution showed a more irregular structure than what was expected from angular data, with the appearance of super-clusters and large voids. This three-dimensional picture no longer showed any clear evidence of homogeneity, in contrast to the angular data. From this discussion, we see that the argument is not strong since it is based on the volume limited three-dimensional samples and the interpretation seems to have been conveniently chosen to support the argument.

Further information on galaxy distribution without involving observations of the redshift is the number count as a function of apparent magnitude and corresponding angular catalogues. The galaxy count as a function of magnitude is one of the very first elements that were studied [24] and gave rise to extensive problems that are still there today. The point is that one can show that the exponent α, which characterizes this counting, is given by $\alpha = \frac{1}{5}F$ (F is the fractal dimension) implying that $\alpha = 0.6$ for a homogeneous distribution and has a smaller value for a fractal one. Unfortunately, the observed behaviour is characterized by $\alpha = 0.6$ for fractal dimensions (small scales) and by $\alpha = 0.4$ for large scales (homogeneous ones). As a way out of that apparent paradox, it has been argued

[22] that fractal correlations can even be over $100h^{-1}Mpc$ from three-dimensional volume limited catalogues. They [22] argue that one must, at small scales, find almost no galaxies because the total number is rather small. Then one enters a regime that is dominated by finite-size fluctuation effects. Finally the correct scaling behaviour of the distribution emerges. This means that if one has a fractal distribution, there will be at first a rise of the conditional density, due to finite size effects because no galaxies are present before a certain characteristic length is reached. Once one enters the correct scaling regime, the density will start to decay according to a power law corresponding to the fractal correlations. In this intermediate regime of rise and fall of the density, there will be a region in which the density can be approximated by a constant value. This region will lead to an apparent dimension $F = 3$ which is not real, but is due to finite size effects.

Another natural question which arises from the above discussion is what happens when a three-dimensional fractal set is projected onto the celestial globe. What does such a projection look like? This question has been addressed by Durrer and Eckman [25] who consider the characteristics of the projected fractal sets, especially their scaling properties. The general theoretical argument leads to the prediction of a homogeneous universe, which has dimension three, while the analysis performed [11] indicates a dimension of two. Their results [25] show that if one takes finite size effects properly into account, one may find that a fractal set of dimension two in three-dimensional space can have a non-fractal and very homogeneous projection onto the celestial globe. Depending on how finite size effects are taken into account, one may find that the projection is sometimes homogeneous and sometimes fractal. It is argued [25] that there is no contradiction between observing a two-dimensional fractal in three-dimensional space and a projection of equal size points

onto a celestial globe. In order to explain the celestial paradox and to put it into context, Durrer and Eckman adapted a mathematical procedure of Hausdorff measure of sets which we outline below:

2.1 Hausdorff Measure of a set

A set $A \subset R^3$ is said to have a Hausdorff dimension d if it can be covered by sets $S_{i,\delta}$ of diameter less than δ in such a way that

$$H^s(A) = \liminf_{\delta \to 0} \sum_i (\text{diameter } S_{i,\delta})^s = \begin{cases} 0 & \text{if } s > d; \\ \infty & \text{if } s < d. \end{cases}$$

For $s = d$, the number $H^d(A)$ is non-negative, possibly infinite, and it is defined to be *Hausdorff measure* of the set A. If d is an integer, and $H^d(A) < \infty$, one can decompose A into a regular part (consisting of piecewise rectifiable sets of dimension d, e.g., lines or sheets) and a singular part (consisting of 'dust'). Almost every projection of the regular part onto a d-dimensional plane is of positive measure, while all projections of the singular part (which is the relevant case for galaxies) have measure zero, i.e., they are very small. Hence the projection from a d-dimensional set A to a two-dimensional space (the celestial globe) is of positive measure, (and hence relatively smooth) only in the case when $d > 2$, or $d = 2$ and either $H^2(A) = \infty$ or A has a regular part, in which case A must contain rectifiable 'sheets'. This case is irrelevant to galaxies, since we consider galaxies to be points or disks in this analysis which, hence, form a dust-like (or singular) set. The above discussion leaves one to wonder if there is any difference between a fractal set and a non-fractal one. This also means that the fractal model believed to hold at large scales of our universe may simply be the usual Friedmann model.

In an analytic universe, isotropy at every point of a system simply implies homogeneity

of the system [10]. This may not be the case in a fractal universe. Now in a fractal universe where we do not make assumptions on the validity of the cosmological principle, how could we solve the Einstein's equation? According to references [26-28], Tolman is one of the prominent researchers who tried to answer this question. He came up with a metric for Einstein's equation for a dust-filled universe with zero pressure. Tolman's metric has a preferred centre (at the point of isotropy) for the universe, so there exists a privileged observer. The earth may be the preferred centre with us as privileged observers. In this case, Tolman's metric is for a universe that is isotropic at one point (i.e., at the center) but inhomogeneous. This means that we are in a privileged position, while a typical place of a galaxy, belonging to the fractal structure, is within a fractal cluster [21]. Tolman's metric therefore, is not consistent with the expectation of a fractal structure. However, up to now, no one has tried to write down a fractal metric and seen how Einstein's equation could be solved for such a metric. Since the dynamics and evolution of our universe can be explained by solving Einstein's equations for a given metric, it is difficult to make predictions in this model and compare these predictions with the observations in our universe. It may therefore, be possible that the fractal model is as a result of misinterpretations of the available observational data for our universe or is a result of the limited samples that have been obtained from the three-dimensional maps of our universe. These maps however, depend on our ability to measure distance. The distance measurements involve a complicated ladder of measurements proceeding from small distances to ever large distances. At each rung of this ladder, some physical assumptions have to be made. In more or less hidden form, the assumption that the universe is Friedmann may enter into these measurements. Let us make the problem posed by these catalogues that involve distance

measurements much clearer by briefly outlining some of the methods used to obtain these distances as below:

2.2 Cosmic Distance Measurements

To illustrate the uncertainties in cosmic distance measurements, we note that the universe is charted with a sequence of techniques each of which takes us out to a greater range of distances [17]. Each level is less reliable than the last, so that there is considerable uncertainty about measurements of very great distances. A common method for distance measurements is the use of parallax.

This is a triangulation using a baseline of length $2d$ that is known. Suppose we have an object that is located at unknown distance D vertically above the midpoint of our baseline. As we move from one end of the baseline to the other, the direction of our object changes.This can be observed as an apparent displacement of our object relative to other objects far more distant whose direction hardly alters (e.g., distant stars). If the angular displacement of our object is 2φ, then by trigonometry,

$$D = \frac{d}{tan\varphi} = \frac{d}{\varphi}$$

since φ is very small in practice. The angle φ is the parallax of our object relative to our baseline. In this way, distance measurements within the solar system can be performed, using baselines on the earth, whose length can be established by direct measurements e.g., radar ranging (measurement of a time delay between the emission of a pulse from one end and its reception after reflection from the other end). The mean earth-sun distance (astronomical unit, $a.u$), provides the scale for the fundamental baseline from which we can step outside our solar system. This baseline is the diameter of the earth's orbit, and

enables the distances of nearer stars to be measured by measuring their parallax after six months using the distant stars (whose parallax is negligible) as background. The basic cosmic distance unit is defined in terms of parallax: one parsec ('parallax-second') is the distance of an object whose parallax φ is one second of arc i.e.,

$$\begin{aligned} 1\text{parsec(pc)} &= \frac{1\text{a.u}}{1'' \text{ in radians}} \\ &= \frac{3600\text{x}180 \text{ a.u}}{\pi} \\ &= 206265 \text{ a.u} \\ &= 3.086\text{x}10^{16}\text{m} \\ &= 3.26 \text{ light} - \text{years}. \end{aligned}$$

We briefly outline some of the methods used to determine cosmic distances below:

2.3 Measurement of Distance using Apparent Luminosity

Suppose we know the absolute luminosity L of a star or a galaxy (the total power radiated by the star or galaxy), and suppose also that the apparent luminosity l (power traveling across unit area at the observer, normal to the line of sight) has been measured, then the inverse square-law for l in terms of L and distance D is given by the conservation of energy as (assuming no absorption in space):

$$L = 4\pi l D^2$$

or

$$D = \sqrt{\frac{L}{4\pi l}}.$$

Thus D can be found from measurements of l, provided L is known.

2.4 Measurement of Distance using Standard Candles (Cepheids)

Astronomers do not use the power l as a measure of apparent brightness but they instead use [17] a logarithmic measure m called the apparent magnitude. The apparent magnitude is defined so that two objects whose luminosities l_1 and l_2 differ by a factor of 100 differ in apparent magnitude by 5, so that

$$\frac{l_1}{l_2} = 100^{(m_2 - m_1)/5}.$$

The absolute magnitude M of an object is the apparent magnitude that the object would have at a distance of $10pc$. Thus, measuring D in pc,

$$l_m \mathrm{x} 4\pi \mathrm{D}^2 = \mathrm{l_M x} 4\pi 10^2.$$

Therefore,

$$100^{(M-m)/5} = \frac{10^2}{D^2}$$

or

$$D = 10^{1+(m-M)/5}$$

so that

$$m - M = 5\, log_{10}\, (\frac{D}{10})$$

where $m - M$ is called the distance modulus. There are certain classes of objects for which we do know M e.g., the Cepheid variables. These are stars that vary [17,1] regularly in brightness, with periods P of the order of days. It was observed by Leavitt in 1912 that M and P are approximately linearly related for the Cepheids in the Small Magellanic Cloud (now known to be the 'satellite' sub-galaxy of our own). Since these stars are all roughly at the same distance from us, she concluded that m was uniquely related to M, and hence M

to P, thus giving an absolute luminosity versus period relation. Because all Cepheids with the same period have the same M, these stars may be employed as 'standard candles' for distance determination, once the relation has been calibrated by M for Cepheids within the galaxy, using a lower level of the distance hierarchy. Thus a Cepheid with period 10 days ($logP = 1$) has an absolute magnitude $M \approx -3$. In the Magellanic Cloud, a physically similar object (same M) has an apparent magnitude m of about 16. Therefore, the distance modulus $m - M$ is about 19, and the distance is

$$D = 10^{1+19/5} pc = 10^{24/5} pc \approx 6\text{x}10^4 \text{pc}.$$

This shows that we are now outside our galaxy whose diameter is about $4\text{x}10^4$pc. Cepheids are intrinsically rather bright (up to $M \approx -6$), and they can be resolved in a number of galaxies as well as our own. However, there are only a few galactic Cepheids in clusters whose distance is known, and this reduces the accuracy of the method.

2.5 Measurement of Distance using Redshift

The present age of the universe is thought to be in the range of ten to twenty billion years. Galaxies were formed when the universe was only a few million years old, and the microwave receivers have been seeing back to a time when the universe was merely a few million years old. There is an important phenomenon that is associated with the fact that we are looking into the past: this is the redshift z of the light from distant objects. Historically, it was noticed that the spectral lines in the spectra of the more distant galaxies were shifted towards longer wavelengths relative to the same lines in the spectra of their nearer counterparts [15]. This redshift was interpreted by Hubble as being due to the Doppler shift and he concluded from his data that the more distant objects were receding from us at greater speeds than the nearby ones, thus giving rise to a greater red-ward shift

of the spectral lines. Mathematically, if v is the speed of the receding galaxy, c the speed of light, D the distance to the galaxy, and $z < 1$, then Hubble law states that

$$v = cz = HD$$

where H is the Hubble constant.

If we consider the fact that light from an Andromeda galaxy left it two million years ago, and an Astronomer photographs it through a telescope, he sees this galaxy as it was two million years ago. Similarly, the light from Vega galaxy left it fifty million years ago, so that a photograph of it now gives us its picture as it was fifty million years back. This is how we obtain a picture of the universe as it was a billion years ago. Photographs of galaxies that are within a distance of hundred million light-years will yield the picture of the expanding universe as it had been during the last hundred million light-years. Since this time is relatively short on a cosmic scale, we can take it to represent the picture of the universe as we see it today. And in the same way we can also regard the Hubble constant derived from this measurement as the Hubble constant at the present time, H_o. If we next extend the measurements out into space, to galaxies whose distance from us is about five hundred million light-years, we can also get the value of H_o within this time of five hundred million light-years. If the accuracy of our measurements permits us to go still further out into space, we can measure galaxies at a period of one billion light-years, and then two billion light-years, and so on. The further out we look into space, the further back we see in time. In this way, we can uncover the state of the expanding universe in earlier epoch. Although the idea behind these measurements look so simple, the measurements are very hard to carry out in practice because it is difficult to measure the distance to remote galaxies with desirable accuracy [29].

We therefore, see that the information given by catalogues involving distance measurements has led to a lot of misunderstanding about the distribution of visible matter in the universe and whether or not our universe can be argument by the Friedmann universe at large scales. From this entire discussion, we see that a lot of research work has been done in this area but none of this has been able to rule out the homogeneous distribution of luminous matter and therefore, establish whether the Friedmann model is valid at large scales or not. There is therefore, need to establish from data involving no distance measurements whether or not our universe is Friedmann at a certain scale and if visible matter is uniformly distributed in it. In the next chapter of this work, the method used in laying the basis for experimental work for satisfactorily answering this question has been clearly discussed .

CHAPTER THREE

3. METHODOLOGY

In trying to answer the question of how much we can learn from astronomical observations that involve no assumptions about the background geometry, three astronomical quantities were considered that can easily be measured. These are:

1. The redshift z, of the light from an astronomical object (star, galaxy, supernova, etc).

2. The light intensity I, from such an object.

3. The number density per solid angle of a given class of objects in a given direction.

We suppose that we are given a large list of all astronomical objects for which the above quantities have been measured together with the direction from which the light comes. How much can we learn just from this data coupled with some plausible assumptions, for instance that the supernova of a given type have constant absolute power?

A first question is whether such data is compatible with the assumption that the universe is described by a Friedmann metric. To answer this question, the functional inter-dependence of these three quantities assuming an underlying Friedmann metric was investigated and the results prepared in a form suitable for comparison with the observed dependencies. Concerning the redshift z, it was assumed that galaxies were uniformly distributed in the universe and that, during the observed time period, new ones do not appear and old ones do not disappear. For each interval $(z,\ z+dz)$ of redshift, the number of galaxies of a given kind were counted with a redshift in that interval, say $n(z)$. Trying to fit this function $n(z)$ to the corresponding counts obtained from observational data by an appropriate choice of parameters, it was possible to judge whether the observations were

compatible with a uniform density of visible matter at some scale in a Friedmann universe. If so, it could also be decided whether the universe is flat, hyperbolic or spherical. It was next assumed that the given large list of astronomical quantities had constant absolute power. It was investigated how the observed light intensity I from them depends on the above redshift, z. Then, it was further investigated whether $\kappa = 0, 1$ or -1. An analytical approach in answering these questions was used, although simple computer programs were also written down for their graphical evaluation.

Since an underlying Friedmann metric was assumed, there was need to derive the Einstein's equations describing the evolution of the universe based on this metric.

3.1 Derivation of Einstein's Equations Based on the Friedmann Metric.

We now derive the Einstein's equations describing the evolution of the universe based on the Friedmann metric. To do this, we need the Γ-symbols of the Friedmann metric. An efficient way of computing them is to consider the functional:

$$l = \int_{\tau_0}^{\tau_1} \left(c^2 \dot{t}^2 - \frac{R^2(t)}{(1+\kappa r^2)^2} (\dot{x}^2 + \dot{y}^2 + \dot{z}^2) \right) d\tau$$

where $r^2 = x^2 + y^2 + z^2$ and the dot above the time or space coordinate denotes differentiation of that coordinate w.r.t τ . The Γ-symbols can be read off from the coefficients of the quadratic terms in the dotted coordinates in the Euler-Lagrange equations:

$$\frac{d}{d\tau}\left(\frac{\partial l}{\partial \dot{t}}\right) = \frac{\partial l}{\partial t}; \quad \frac{d}{d\tau}\left(\frac{\partial l}{\partial \dot{x}}\right) = \frac{\partial l}{\partial x}$$

and

$$\frac{d}{d\tau}\left(\frac{\partial l}{\partial \dot{y}}\right) = \frac{\partial l}{\partial y}; \quad \frac{d}{d\tau}\left(\frac{\partial l}{\partial \dot{z}}\right) = \frac{\partial l}{\partial z}.$$

As an example, let us calculate the Γ-symbols that can be obtained from the first of these equations:

$$\frac{d}{d\tau}\left(2c^2\dot{t}\right) = \frac{-2R(t)R'(t)}{(1+\kappa r^2)^2}(\dot{x}^2+\dot{y}^2+\dot{z}^2)$$

where $R'(t) = \frac{dR}{dt}$. This equation yields

$$2c^2\ddot{t} + \frac{2R(t)R'(t)}{(1+\kappa r^2)^2}(\dot{x}^2+\dot{y}^2+\dot{z}^2) = 0$$

or

$$\ddot{t} + \frac{R(t)R'(t)}{c^2(1+\kappa r^2)^2}(\dot{x}^2+\dot{y}^2+\dot{z}^2) = 0\,,$$

which is the t-component of the geodesic equation,

$$\ddot{x}^\mu + \Gamma^\mu{}_{\rho\sigma}\dot{x}^\rho\dot{x}^\sigma = 0\,.$$

The non-vanishing Γ-symbols of the form $\Gamma^0{}_{\rho\sigma}$ are therefore:

$$\Gamma^0{}_{11} = \Gamma^0{}_{22} = \Gamma^0{}_{33} = \frac{R(t)R'(t)}{c^2(1+\kappa r^2)^2}\,.$$

Similarly, the non-vanishing Γ-symbols obtained from the remaining Euler-Lagrange equations can be shown to be:

$$\Gamma^1{}_{10} = \Gamma^1{}_{01} = \Gamma^2{}_{20} = \Gamma^2{}_{02} = \Gamma^3{}_{30} = \Gamma^3{}_{03} = \frac{R'(t)}{R(t)}$$

$$\Gamma^1{}_{11} = \Gamma^2{}_{21} = \Gamma^2{}_{12} = \Gamma^3{}_{31} = \Gamma^3{}_{13} = \frac{-2\kappa x}{1+\kappa r^2}$$

$$\Gamma^1{}_{12} = \Gamma^1{}_{21} = \Gamma^2{}_{22} = \Gamma^3{}_{32} = \Gamma^3{}_{23} = \frac{-2\kappa y}{1+\kappa r^2}$$

$$\Gamma^1{}_{13} = \Gamma^1{}_{31} = \Gamma^2{}_{23} = \Gamma^2{}_{32} = \Gamma^3{}_{33} = \frac{-2\kappa z}{1+\kappa r^2}$$

$$\Gamma^1{}_{22} = \Gamma^1{}_{33} = \frac{2\kappa x}{1+\kappa r^2}$$

$$\Gamma^2{}_{11} = \Gamma^2{}_{33} = \frac{2\kappa y}{1+\kappa r^2}$$
$$\Gamma^3{}_{11} = \Gamma^3{}_{22} = \frac{2\kappa z}{1+\kappa r^2}$$

In order to derive the Einstein equations, we first need to calculate the Ricci tensor $R_{\alpha\beta}$, defined as

$$R_{\alpha\beta} = R^{\mu}{}_{\alpha\mu\beta} \ ,$$

where $R^{\mu}{}_{\alpha\nu\beta}$ are the components of the Riemann tensor. By definition of the Riemann curvature, we know that

$$R(X,Y,Z) = \nabla_X(\nabla_Y Z) - \nabla_Y(\nabla_X Z) - \nabla_{[X,Y]}Z$$

or, expressed in terms of components,

$$\begin{aligned} R^{\mu}{}_{\nu\rho\sigma}\frac{\partial}{\partial x^\mu} &= R\left(\frac{\partial}{\partial x^\rho}, \frac{\partial}{\partial x^\sigma}, \frac{\partial}{\partial x^\nu}\right) \\ &= \nabla_{\frac{\partial}{\partial x^\rho}}\left(\nabla_{\frac{\partial}{\partial x^\sigma}}\frac{\partial}{\partial x^\nu}\right) - \nabla_{\frac{\partial}{\partial x^\sigma}}\left(\nabla_{\frac{\partial}{\partial x^\rho}}\frac{\partial}{\partial x^\nu}\right) - \nabla_{\left[\frac{\partial}{\partial x^\rho}, \frac{\partial}{\partial x^\sigma}\right]}\frac{\partial}{\partial x^\nu} \ . \end{aligned}$$

The last term is zero since the Lie bracket of coordinate vector fields vanishes. Applying the definition

$$\nabla_{\frac{\partial}{\partial x^\alpha}}\frac{\partial}{\partial x^\beta} = \Gamma^{\rho}{}_{\alpha\beta}\frac{\partial}{\partial x^\rho}$$

to the terms in brackets we have

$$\begin{aligned} R^{\mu}{}_{\nu\rho\sigma}\frac{\partial}{\partial x^\mu} &= \nabla_{\frac{\partial}{\partial x^\rho}}\left[\Gamma^{\alpha}{}_{\sigma\nu}\frac{\partial}{\partial x^\alpha}\right] - \nabla_{\frac{\partial}{\partial x^\sigma}}\left[\Gamma^{\alpha}{}_{\rho\nu}\frac{\partial}{\partial x^\alpha}\right] \\ &= \left(\frac{\partial}{\partial x^\rho}\Gamma^{\alpha}{}_{\sigma\nu}\right)\frac{\partial}{\partial x^\alpha} + \Gamma^{\alpha}{}_{\sigma\nu}\Gamma^{\beta}{}_{\rho\alpha}\frac{\partial}{\partial x^\beta} - \left(\frac{\partial}{\partial x^\sigma}\Gamma^{\alpha}{}_{\rho\nu}\right)\frac{\partial}{\partial x^\alpha} \\ &\quad - \Gamma^{\alpha}{}_{\rho\nu}\Gamma^{\beta}{}_{\sigma\alpha}\frac{\partial}{\partial x^\beta} \ . \end{aligned}$$

Replacing α by μ in the first and third terms, and β by μ in the second and last terms, we obtain

$$R^{\mu}{}_{\nu\rho\sigma}\frac{\partial}{\partial x^\mu} = \left(\frac{\partial}{\partial x^\rho}\Gamma^{\mu}{}_{\sigma\nu}\right)\frac{\partial}{\partial x^\mu} + \Gamma^{\alpha}{}_{\sigma\nu}\Gamma^{\mu}{}_{\rho\alpha}\frac{\partial}{\partial x^\mu} - \left(\frac{\partial}{\partial x^\sigma}\Gamma^{\mu}{}_{\rho\nu}\right)\frac{\partial}{\partial x^\mu} - \Gamma^{\alpha}{}_{\rho\nu}\Gamma^{\mu}{}_{\sigma\alpha}\frac{\partial}{\partial x^\mu} \ .$$

Reading off ${R^{\mu}}_{\nu\rho\sigma}$ from the above equation and replacing ρ by μ we get:

$$R^{\mu}{}_{\nu\mu\sigma} = R_{\nu\sigma} = \frac{\partial}{\partial x^{\mu}}\Gamma^{\mu}{}_{\sigma\nu} + \Gamma^{\mu}{}_{\sigma\nu}\Gamma^{\alpha}{}_{\mu\alpha} - \frac{\partial}{\partial x^{\sigma}}\Gamma^{\mu}{}_{\mu\nu} - \Gamma^{\alpha}{}_{\mu\nu}\Gamma^{\mu}{}_{\sigma\alpha}\,.$$

If we now replace σ by β, ν by α and α by γ we get:

$$R_{\alpha\beta} = \Gamma^{\mu}{}_{\beta\alpha,\mu} + \Gamma^{\mu}{}_{\beta\alpha}\Gamma^{\gamma}{}_{\mu\gamma} - \Gamma^{\mu}{}_{\mu\alpha,\beta} - \Gamma^{\mu}{}_{\beta\gamma}\Gamma^{\gamma}{}_{\mu\alpha}$$

where ${\Gamma^{\rho}}_{\alpha\beta,\sigma}$ denotes $\frac{\partial}{\partial x^{\sigma}}{\Gamma^{\rho}}_{\alpha\beta}$. For $\mu, \alpha, \beta, \gamma = 0, 1, 2, 3$ and $\alpha = \beta = 1$, we obtain:

$$R_{11} = \Gamma^{\mu}{}_{11,\mu} + \Gamma^{\mu}{}_{11}\Gamma^{\gamma}{}_{\mu\gamma} - \Gamma^{\mu}{}_{\mu1,1} - \Gamma^{\mu}{}_{1\gamma}\Gamma^{\gamma}{}_{\mu1}\,. \tag{4}$$

For the first term on the R.H.S of equation (4) we have

$$\begin{aligned}\Gamma^{\mu}{}_{11,\mu} &= \Gamma^{0}{}_{11,0} + \Gamma^{1}{}_{11,1} + \Gamma^{2}{}_{11,2} + \Gamma^{3}{}_{11,3} \\ &= \frac{\partial}{\partial x}\left(\frac{-2\kappa x}{1+\kappa r^2}\right) + \frac{\partial}{\partial y}\left(\frac{2\kappa y}{1+\kappa r^2}\right) + \frac{\partial}{\partial z}\left(\frac{2\kappa z}{1+\kappa r^2}\right) \\ &+ \frac{\partial}{\partial t}\left(\frac{R(t)R'(t)}{c^2(1+\kappa r^2)^2}\right) = \frac{R(t)R''(t) + R'^2(t)}{c^2(1+\kappa r^2)^2} \\ &+ \frac{2\kappa}{(1+\kappa r^2)} + \frac{4\kappa^2(x^2 - y^2 - z^2)}{(1+\kappa r^2)^2}\,.\end{aligned} \tag{5}$$

Similarly the remaining terms are calculated and found to be:

$$\Gamma^{\mu}{}_{11}\Gamma^{\gamma}{}_{\mu\gamma} = \frac{3R'^2(t)}{c^2(1+\kappa r^2)^2} + \frac{12\kappa^2(x^2 - y^2 - z^2)}{(1+\kappa r^2)^2} \tag{6}$$

$$\Gamma^{\mu}{}_{\mu1,1} = \frac{-6\kappa}{(1+\kappa r^2)} + \frac{12\kappa^2 x^2}{(1+\kappa r^2)^2} \tag{7}$$

$$\Gamma^{\mu}{}_{1,\gamma}\Gamma^{\gamma}{}_{\mu,1} = \frac{2R'^2(t)}{c^2(1+\kappa r^2)^2} + \frac{2k^2x^2}{(1+\kappa r^2)^2} - \frac{8\kappa^2(y^2+z^2)}{c^2(1+\kappa r^2)^2}\,. \tag{8}$$

Substituting equations (5), (6), (7) and (8) into equation (4), we obtain the component of the Ricci tensor R_{11} as

$$R_{11} = \frac{R(t)R''(t) + 2R'^2(t) + 8\kappa^2c^2}{c^2(1+\kappa r^2)^2}\,.$$

In the same manner, it can be shown that the other non-vanishing values are R_{22}, R_{33} and R_{00} with

$$R_{33} = R_{22} = R_{11} = \frac{R(t)R''(t) + 2R'^2(t) + 8\kappa^2 c^2}{c^2(1+\kappa r^2)^2}$$

and

$$R_{00} = \frac{-3R''(t)}{R(t)} .$$

Now raising the first of the indices of $R_{\alpha\beta}$ we have

$$R^0{}_0 = \frac{-3R''(t)}{c^2 R(t)}$$

and

$$R^1{}_1 = R^2{}_2 = R^3{}_3 = -\frac{\left(8\kappa c^2 + R(t)R''(t) + 2R'^2(t)\right)}{c^2 R^2(t)} .$$

Raising also the second index, we have

$$R^{00} = \frac{-3R''(t)}{c^4 R(t)} \tag{9}$$

and

$$R^{11} = R^{22} = R^{33} = \frac{(1+\kappa r^2)^2\left(8\kappa c^2 + R(t)R''(t) + 2R'^2(t)\right)}{c^2 R^4(t)} .$$

Therefore, the curvature scalar is:

$$R = R^\mu{}_\mu = -6\frac{\left(4\kappa c^2 + R(t)R''(t) + R'^2(t)\right)}{c^2 R^2(t)} . \tag{10}$$

Finally we can now define the Einstein tensor $G^{\mu\nu}$ as:

$$G^{\mu\nu} = R^{\mu\nu} - \frac{1}{2} R\, g^{\mu\nu} . \tag{11}$$

The isotropy requires that the matter content in the universe must be at rest with respect to coordinates x, y, z, since otherwise the direction of the velocity would break the isotropy.

Furthermore, if the universe is assumed to be homogeneous, this matter content must be uniformly distributed everywhere. Recall from the relativistic theory of fields and matter (Noether theory of conservation) that, with every distribution of matter and fields, there is associated a conserved tensor, i.e., the energy-momentum tensor, $T^{\mu\nu}$. The equivalence principle asserts that it is covariantly conserved as is also the Einstein tensor. The component T^{00} is the energy density while the components T^{10}, T^{20}, T^{30} are the momenta densities. The corresponding space components represent the current densities. However, in general, Noether theory does not necessarily lead to a symmetric energy-momentum tensor $T^{\mu\nu}$, but there is always a modification of it which is symmetric, i.e., $T^{\mu\nu} = T^{\nu\mu}$. But from equation (1), the Einstein tensor is related to the symmetric stress-energy tensor of the matter content in the universe by the Einstein equation:

$$G^{\mu\nu} = BT^{\mu\nu}$$

where B as defined earlier is given in terms of the gravitational constant G by $B = 8\pi G c^{-4}$. This tensor is uniform everywhere on a timeslice, i.e., must not depend on the coordinates x, y, z. This implies that the stress-energy tensor must take the form:

$$T^{00} = \rho(t) \tag{12}$$

and

$$T^{11} = T^{22} = T^{33} = \frac{(1 + \kappa r^2)^2 \, p(t)}{R^2(t)}, \tag{13}$$

where $\rho(t)$ and $p(t)$ are the mass density and pressure (both functions of time), respectively. Equation (1) contains two independent equations: one for $\mu = \nu = 0$ and another one for $\mu = \nu = 1, 2, 3$. Using equations (9) and (10) in equation (11), we can easily show that for

$\mu = \nu = 0$,

$$G^{00} = 3\frac{(4\kappa c^2 + R'^2(t))}{c^4 R^2(t)} \,. \tag{14}$$

Now using equations (12) and (14) in equation (1) we get the first equation:

$$12\kappa c^2 + 3R'^2(t) = Bc^4 R^2(t)\rho(t) \,. \tag{2}'$$

Similarly from equation (1) it can be shown that for $\mu = \nu = 1, 2, 3$;

$$G^{11} = G^{22} = G^{33} = -\frac{(1 + \kappa r^2)\Big(4\kappa c^2 + 2R(t)R''(t) + R'^2(t)\Big)}{c^2 R^4(t)} \,. \tag{15}$$

Substituting equations (2)′ and (13) into equation (1) we get the second equation:

$$4\kappa c^2 + 2R(t)R''(t) + R'^2(t) = -Bc^2 R^2(t)p(t) \,. \tag{3}'$$

Note that equations (2)′ and (3)′ are just the ealier written down equations (2) and (3) respectively.

In the next chapter, these derived Einstein's equations will be used to study the inter-dependence between the above mentioned astronomical quantities and also to address other already mentioned questions.

CHAPTER FOUR

4. DISCUSSION AND RESULTS

4.1 Introduction

In the last chapter, an efficient way was given of obtaining the Einstein's equations that would best describe the evolution of our universe starting from the functional:

$$l = \int_{\tau_0}^{\tau_1} \left(c^2 \dot{t}^2 - \frac{R^2(t)}{(1+\kappa r^2)^2} (\dot{x}^2 + \dot{y}^2 + \dot{z}^2) \right) d\tau.$$

In this chapter, we shall make use of those Einstein's equations to investigate the inter-relationships between the redshift z of light from a given object; the light intensity I from a given object (e.g., a galaxy or a supernova), and the number density per solid angle of a given class of objects in a given direction.

4.2 Relation Between the Number Density of Galaxies and the Redshift

We now investigate the relation between the redshift z and the number density of galaxies observed at that redshift by assuming that galaxies of a given type are homogeneously distributed in the universe and do not appear and disappear within the time span of interest. For each interval $[z,\ z+dz]$ of redshift, we count how many galaxies of that kind we see with a redshift in that interval, say $n(z)dz$.

The above derived equations $(2)'$ and $(3)'$ imply an energy conservation law: differentiating equation $(2)'$ w.r.t time t and multiplying the result by $R(t)$ we get:

$$6R(t)R'(t)R''(t) = 2Bc^4R^2(t)R'(t)\rho(t) + Bc^4R^3(t)\rho'(t)\ . \tag{16}$$

Multiplying equation $(3)'$ by 3 and re-arranging it we get:

$$6R(t)R''(t) = -\big(12\kappa c^2 + 3R'^2(t)\big) - 3Bc^2R^2(t)p(t)\ .$$

If we substitute equation $(2)'$ into this equation and multiply the result by $R'(t)$, we get:

$$6R(t)R'(t)R''(t) = -Bc^4R'(t)R^2(t)\rho(t) - 3Bc^2R'(t)R^2(t)p(t)\,. \tag{17}$$

If we finally subtract equation (17) from equation (16), we can write the end result in the form:

$$\frac{d}{dt}\left(\rho(t)c^2R^3(t)\right) = -p(t)\frac{d}{dt}R^3(t)\,. \tag{18}$$

So the rate of change of energy in the universe is the negative of the product of the pressure and the rate of change of the volume in the universe. The universe as we see it today seems to be matter-dominated. This matter seems to be concentrated in galaxies that are uniformly distributed and are at rest w.r.t t=constant hypersurfaces. This matter, e.g. galaxies, can therefore be regarded, as 'atoms' of a gas at zero temperature. The equation of state of such a gas is simply $p(t) = 0$. From equation (18), it is clear that the conservation law for the stress energy tensor $T^{\mu\nu}$ for $p(t) = 0$, says that the total mass contained in the universe remains constant, i.e., the mass density times the radius of the universe cubed is a constant say, α:

$$\rho(t)R^3(t) = \alpha\,. \tag{19}$$

If we substitute equation (19) into equation $(2)'$ we get

$$12\kappa c^2 + 3R'^2(t) = \frac{Bc^4\alpha}{R(t)}$$

or

$$R'(t) = \sqrt{\frac{Bc^4\alpha}{3R(t)} - 4\kappa c^2}$$

implying that

$$dt = \frac{dR}{\sqrt{\frac{Bc^4\alpha}{3R} - 4\kappa c^2}}\,. \tag{20}$$

Now consider an emitted light ray that starts at $r(t_e)$ and travels towards the origin such that at time $t = t_o$ it reaches the origin, i.e., $r(t_o) = 0$. Parameterize its null geodesic in spherical coordinates as follows:

$$x(\tau) = r(\tau)\sin\theta\cos\varphi$$

$$y(\tau) = r(\tau)\sin\theta\sin\varphi$$

$$z(\tau) = r(\tau)\cos\theta$$

for some fixed θ, φ . It follows that

$$\dot{x}^2 + \dot{y}^2 + \dot{z}^2 = \dot{r}^2 \ .$$

Then the fact that we are considering a null geodesic implies that

$$c^2\dot{t}^2 - \frac{R^2\dot{r}^2}{(1+\kappa r^2)^2} = 0,$$

or

$$c\dot{t} = \pm\frac{R(t)\dot{r}}{1+\kappa r^2} \ .$$

But $\dot{t}$ is positive while $\dot{r}$ is negative by our assumption, hence

$$cdt = -\frac{R(t)dr}{1+\kappa r^2} \ .$$

Rearranging this equation and integrating, we have

$$\int_{t_e}^{t_o} \frac{c}{R(t)}\,dt = -\int_{r(t_e)}^{r(t_o)} \frac{1}{1+\kappa r^2}\,dr \ . \tag{21}$$

Using equation (17) in equation (18) to change to integration over R, we have

$$\int_{R(t_e)}^{R(t_o)} \frac{c}{\sqrt{R}\sqrt{\frac{Bc^4\alpha}{3} - 4\kappa c^2 R}}\,dR = -\int_{r(t_e)}^{r(t_o)} \frac{1}{1+\kappa r^2}\,dr \ . \tag{22}$$

We solve equation (22) for three cases:

1. case $1 : \kappa = 0$.

In this case, equation (22) becomes

$$\int_{R(t_e)}^{R(t_o)} \frac{c}{\sqrt{R}\sqrt{\frac{Bc^4\alpha}{3}}}\, dR = -\int_{r(t_e)}^{r(t_o)} dr \ ,$$

which can be integrated easily to give:

$$-r(t_o) + r(t_e) = \sqrt{\frac{12R(t_o)}{Bc^2\alpha}} - \sqrt{\frac{12R(t_e)}{Bc^2\alpha}} \ . \tag{23}$$

But the redshift equation is given by

$$z = \frac{R(t_o)}{R(t_e)} - 1$$

or

$$R(t_e) = \frac{R(t_o)}{1+z} \ . \tag{24}$$

If we now use equation (24) in equation (23) and set $r(t_o) = 0$, we have

$$r(t_e) = \sqrt{\frac{12R(t_o)}{Bc^2\alpha}} - \sqrt{\frac{12R(t_o)}{Bc^2\alpha(1+z)}} \ . \tag{25}$$

2. case $2 : \kappa = 1$.

In this case, equation (22) becomes:

$$\int_{R(t_e)}^{R(t_o)} \frac{c}{\sqrt{R}\sqrt{\frac{Bc^4\alpha}{3} - 4c^2R}}\, dR = -\int_{r(t_e)}^{r(t_o)} \frac{1}{1+\ r^2}\, dr \ . \tag{26}$$

Integrating the R.H.S of this equation and letting $r(t_o) = 0$ gives

$$\tan^{-1} r(t_e)$$

while the L.H.S is solved by letting $R = \frac{Bc^2\alpha \sin^2\theta}{12}$, hence $dR = \frac{Bc^2\alpha}{6} \sin\theta \cos\theta \, d\theta$. Using this substitution for the L.H.S, the above integral yields the result:

$$\tan^{-1} r(t_e) = \sin^{-1}\left(\sqrt{\frac{12R(t_o)}{Bc^2\alpha}}\right) - \sin^{-1}\left(\sqrt{\frac{12R(t_e)}{Bc^2\alpha}}\right).$$

Using equation (24) we have this result as

$$\tan^{-1} r(t_e) = \sin^{-1}\left(\sqrt{\frac{12R(t_o)}{Bc^2\alpha}}\right) - \sin^{-1}\left(\sqrt{\frac{12R(t_o)}{Bc^2\alpha(1+z)}}\right). \tag{27}$$

Taking tangent of both sides of equation (27) and using the identity

$$\tan(A \pm B) = \frac{\tan A \pm \tan B}{1 \mp \tan A \tan B},$$

we have

$$r(t_e) = \frac{\tan\sin^{-1}\left(\sqrt{\frac{12R(t_o)}{Bc^2\alpha}}\right) - \tan\sin^{-1}\left(\sqrt{\frac{12R(t_o)}{Bc^2\alpha(1+z)}}\right)}{1 + \tan\sin^{-1}\left(\sqrt{\frac{12R(t_o)}{Bc^2\alpha}}\right)\tan\sin^{-1}\left(\sqrt{\frac{12R(t_o)}{Bc^2\alpha(1+z)}}\right)}. \tag{28}$$

Using the trigonometric identities:

$$\begin{aligned}\tan &= \frac{\sin}{\cos} \\ &= \frac{\sin}{\sqrt{(1-\sin^2)}}\end{aligned}$$

and simplifying, equation (28) reduces to the form:

$$r(t_e) = \frac{\sqrt{12R(t_o)}\left[\sqrt{Bc^2\alpha(1+z) - 12R(t_o)} - \sqrt{Bc^2\alpha - 12R(t_o)}\right]}{\sqrt{Bc^2\alpha - 12R(t_o)}\,\sqrt{Bc^2\alpha(1+z) - 12R(t_o)} + 12R(t_o)}. \tag{29}$$

3. case 3 : $\kappa = -1$.

This case reduces equation (22) to the form:

$$\int_{R(t_e)}^{R(t_o)} \frac{c\,dR}{\sqrt{R}\,\sqrt{\frac{Bc^4\alpha}{3} + 4c^2R}} = -\int_{r(t_e)}^{r(t_o)} \frac{dr}{1 - r^2}. \tag{30}$$

On substituting $r = \tanh^2\theta$; $r(t_o) = 0$; $R = \frac{Bc^2\alpha \sinh^2\theta}{12}$ and therefore,

$$dR = Bc^2\alpha \sinh\theta \cosh\theta \, d\theta \; ;$$

we have equation (30) as:

$$\tanh^{-1} r(t_e) = \sinh^{-1}\left(\sqrt{\frac{12R(t_o)}{Bc^2\alpha}}\right) - \sinh^{-1}\left(\sqrt{\frac{12R(t_o)}{Bc^2\alpha(1+z)}}\right) . \tag{31}$$

Taking the hyperbolic tangent of both sides of equation (31) and using the identities:

$$\tanh(A \pm B) = \frac{\tanh A \pm \tanh B}{1 \pm \tanh A \tanh B}$$

and

$$\begin{aligned} \tanh &= \frac{\sinh}{\cosh} \\ &= \frac{\sinh}{\sqrt{1+\sinh^2}} , \end{aligned}$$

we can reduce equation (31) in a similar manner as for case 2 to the final form:

$$r(t_e) = \frac{\sqrt{12R(t_o)}\left[\sqrt{Bc^2\alpha(1+z)+12R(t_o)} - \sqrt{Bc^2\alpha+12R(t_o)}\right]}{\sqrt{Bc^2\alpha+12R(t_o)}\,\sqrt{Bc^2\alpha(1+z)+12R(t_o)} - 12R(t_o)} . \tag{32}$$

Equations (25), (29) and (32) can be written as one compact equation in terms of κ as:

$$r(t_e) = \frac{\sqrt{12R(t_o)}\left[\sqrt{Bc^2\alpha(1+z)-12\kappa R(t_o)} - \sqrt{Bc^2\alpha-12\kappa R(t_o)}\right]}{\sqrt{Bc^2\alpha-12\kappa R(t_o)}\,\sqrt{Bc^2\alpha(1+z)-12\kappa R(t_o)} + 12\kappa R(t_o)} . \tag{33}$$

Since t_e itself depends on z, let us henceforth consider $r(t_e)$ as a function $r(z)$ and define $a := Bc^2\alpha - 12\kappa R(t_o)$ and $b := Bc^2\alpha(1+z) - 12R(t_o)$. In this case, equation (33) can be written as:

$$r(z) = \frac{\sqrt{12R(t_o)}\,(\sqrt{b}-\sqrt{a})}{\sqrt{a}\,\sqrt{b}+12\kappa R(t_o)} . \tag{34}$$

For small z, this equation can be expanded as follows: we can write $b = a + Bc^2\alpha z$, hence $\sqrt{b} = \sqrt{a}\sqrt{1 + \frac{Bc^2\alpha}{a} z}$. For small z, we have the following expansion:

$$\sqrt{1 + \frac{Bc^2\alpha}{a} z} = 1 + \frac{1}{2}\frac{Bc^2\alpha}{a} z - \frac{1}{8}\frac{(Bc^2\alpha)^2}{a^2} z^2 + - - - .$$

Therefore,

$$\sqrt{b} = \sqrt{a} + \frac{1}{2}\frac{Bc^2\alpha}{\sqrt{a}} z - \frac{1}{8}\frac{(Bc^2\alpha)^2}{(\sqrt{a})^3} z^2 + - - - . \tag{35}$$

Substituting equation (35) into equation (34) (considering the first two terms of the expansion), and simplifying for very small z, we have

$$r(z) \approx \frac{\sqrt{3R(t_o)/a}}{a + 12\kappa R(t_o)} Bc^2\alpha\, z = \sqrt{\frac{3R(t_o)}{a}}\, z\,,$$

hence $r(z)$ is proportional to z . For small values of z, the speed v of a galaxy receding from us is related to the redshift z by $v = cz$, where c is the speed of light. But we also recall that the same speed v of recession of a galaxy is proportional to its distance D from us by $v = HD$, where H is the hubble constant. From the two above equations of v, we clearly see that $D = \frac{c}{H} z$, hence D is proportional to z.

Similarly, for large values of z, $a <<< b$; $12\kappa R(t_o) <<< \sqrt{ab}$; $12\kappa R(t_o) <<< Bc^2\alpha z$ and $1 <<< z$ so that $r(z)$ is just a constant given as:

$$r(z) \approx \sqrt{\frac{12R(t_o)}{a}}\,.$$

By differentiating equation (33) w.r.t z and simplifying we have:

$$\frac{dr}{dz} = \frac{(Bc^2\alpha)^2\sqrt{3R(t_o)}}{\sqrt{b}\left(\sqrt{a}\,\sqrt{b} + 12\kappa R(t_o)\right)^2}\,. \tag{36}$$

Let N denote the number of galaxies per unit volume of the space with metric

$$\frac{dr^2 + r^2 d\theta^2 + r^2 \sin^2\theta d\varphi^2}{(1 + \kappa r^2)^2}$$

on which the time slices are argument. The volume element is $\frac{r^2 \sin\theta \, d\theta \, d\varphi \, dr}{(1+\kappa r^2)^3}$, hence the number of galaxies between r and dr is given by $\frac{4\pi r^2 dr}{(1+\kappa r^2)^3} \; N$. Our assumption of the number of galaxies enclosed between the coordinate hyperspheres $r(z)$ and $r(z+dz)$ is therefore given by:

$$n(z)dz = \frac{4\pi r^2(z)}{\left(1+\kappa r^2(z)\right)^3} \, N r'(z) dz \; . \tag{37}$$

If we substitute equation (36) and (33) into equation (37) we get:

$$n(z) = \frac{48\pi N R(t_o)(Bc^2\alpha)^2 \sqrt{3R(t_o)}(\sqrt{b}-\sqrt{a})^2}{\left[1+\kappa\left(\frac{(\sqrt{b}-\sqrt{a})}{(\sqrt{ab}+12\kappa R(t_o))}\right)^2\right]^3 [\sqrt{ab}+12\kappa R(t_o)]^4} \; . \tag{38}$$

4.3 Dependence of the Light Intensity on the Redshift

We next consider the relationship between the light intensity I from an emitting star and the redshift z. We consider a star emitting light at an absolute power, L. Let the star be situated at the coordinate $r = 0$. At time $t = t_e$, we consider the light emitted during an interval of time, dt_e. Suppose that, at time $t = t_o$, an observer measures the brightness I of that light which he receives at a redshift z, then his position of reception of the light is given by equation (33). This is because equation (33) is invariant under time reversal i.e., the equation

$$c\dot{t} = \pm \frac{R(t)\dot{r}}{1+\kappa r^2}$$

does not change if we replace t by $-t$. This light that was emitted in the time interval $[t_e, \; t_e + dt_e]$ will pass the observer in the time interval $[t_o, \; t_o + dt_o]$. During this process, what is conserved as the radiation passes through the universe is the number of photons. But each of these photons is red-shifted, hence its energy is reduced by a factor $\frac{1}{1+z}$. Since this red-shifting is for all photons, it means that the energy that passes through the sphere

of radius $r = r(z)$ during the interval $[t_o,\ t_o + dt_o]$ is the same as $\frac{1}{1+z}$ times the energy emitted during the interval $[t_e,\ t_e + dt_e]$. This implies that:

$$I = \frac{L\, dt_e}{(1+z)dt_o\, S_{r(z)}}\ , \tag{39}$$

where $S_{r(z)}$ denotes the surface area of the sphere of radius $r = r(z)$ at time $t = t_o$. But light is described by a null geodesic of the Robertson-Walker metric given by:

$$\frac{c\dot{t}}{R(t)} = \frac{\dot{r}}{1+\kappa r^2}\ . \tag{40}$$

Integrating the L.H.S of equation (40) from time t_e of emission to time t_o of observation and the R.H.S from the coordinate radius $r = 0$ to $r = r(z)$ we have:

$$\int_{t_e}^{t_o} \frac{c}{R(t)}\, dt = \int_0^{r(z)} \frac{1}{1+\kappa r^2}\, dr\ . \tag{41}$$

Equation (41) can be written in terms of the time intervals as:

$$\int_{t_e+dt_e}^{t_o+dt_o} \frac{c}{R(t)}\, dt = \int_0^{r(z)} \frac{1}{1+\kappa r^2}\, dr\ . \tag{42}$$

Applying the fundamental theorem of integral calculus to equation (42) we have

$$\frac{cdt_o}{R(t_o)} - \frac{cdt_e}{R(t_e)} + \int_{t_e}^{t_o} \frac{c}{R(t)}\, dt = \int_0^{r(z)} \frac{1}{1+\kappa r^2}\, dr\ . \tag{43}$$

If we substitute equation (41) into equation (43) we get:

$$\frac{dt_o}{R(t_o)} = \frac{dt_e}{R(t_e)}$$

or

$$\frac{dt_e}{dt_o} = \frac{R(t_e)}{R(t_o)} = \frac{1}{1+z}\ . \tag{44}$$

Substituting equation (44) into equation (39) and noting that the surface area of the sphere $S_{r(z)}$ is given by $\frac{4\pi r^2(z)R^2(t_o)}{\left(1+\kappa r^2(z)\right)^2}$ we get:

$$I = \frac{L\left(1+\kappa r^2(z)\right)^2}{(1+z)^2\ 4\pi r^2(z)R^2(t_o)}\ . \tag{45}$$

Considering small values of z, we have $z <<< 1$ so that $1+\kappa r(z) \approx 1$ and $1+z \approx 1$. Using these approximations in equation (45) and noting that $r(z)$ is proportional to z for small z, we obtain

$$I \approx \frac{L}{4\pi R^2(t_o)\ z^2}\ .$$

But we showed that the distance D is proportional to the redshift z and from our classical expectation, I should be inversely proportional to D^2, hence, I should be inversely proportional to z^2. So our above result of

$$I \approx \frac{L}{4\pi R^2(t_o)\ z^2}$$

agrees with our classical expectation. This implies that the light intensity from nearby galaxies (small values of z) obeys Newtonian physics in which the intensity falls as the inverse of the square of the redshift z. For galaxies which are far away (large values of z), we use the result derived from equation (33), that is, $r(z) \approx \sqrt{\frac{12R(t_o)}{a}}$. If we use this result in equation (45) together with the fact that $z >>> 1$, we get

$$I = \frac{L(1+12\kappa R(t_o)/a)^2}{4\pi R^2(t_o)\ z^2}.$$

According to this result, we see that the intensity I, from far off galaxies also falls as the inverse of z^2 and $r(z)$ grows to some infinite extent.

4.4 Graphical Evaluation of the Results

In the last section of this chapter, we obtained (analytically) the formula that shows us the inter-dependence of the three astronomical quantities i.e., the redshift z, the light intensity I, and the number density $n(z)$ per solid angle of a given class of objects (e.g., galaxies or supernova of a given type) in a given direction. In this section, we write simple computer programs for the graphical evaluation of the results for the number density $n(z)$ versus redshift z and for the intensity I versus redshift z.

1. Light Intensity.

As already discussed above, the intensity I is inversely proportional to the square of the redshift z for both small and large values of z. But from the above derived equations for small and large values of z, we see that as $z \to 0$, $I \to \infty$. To avoid this singularity in our Pascal program, we multiply both sides of equation (45) by z^2 to get

$$z^2 I = \frac{L\left(1+\kappa r^2(z)\right)^2 z^2}{(1+z)^2\, 4\pi r^2(z) R^2(t_o)},$$

where L is the constant absolute power emitted by the given objects while other parameters remain as defined in chapter three. We now write a Pascal program (named intensity as shown in appendix 1) that draws curves of light intensity times z^2 ,i.e, $z^2 I$ against redshift z based on the above equation. Since we are mainly interested in the choice of the parameters ρ and $R(t_o)$ that would give us the shape of the curve that would fit the experimental result from data involving no distance measurements, we can assign other parameters certain constant values e.g., we can assign the number N of galaxies per unit volume of our metric the value 1 and similarly the constant absolute power L can also be assigned the value 1. If we run our program for various values of $R(t_o)$(m) and ρ(kgm^{-3}),

various curves result (see figures 1-6 below):

Figure 1:- z^2 times Intensity versus Redshift

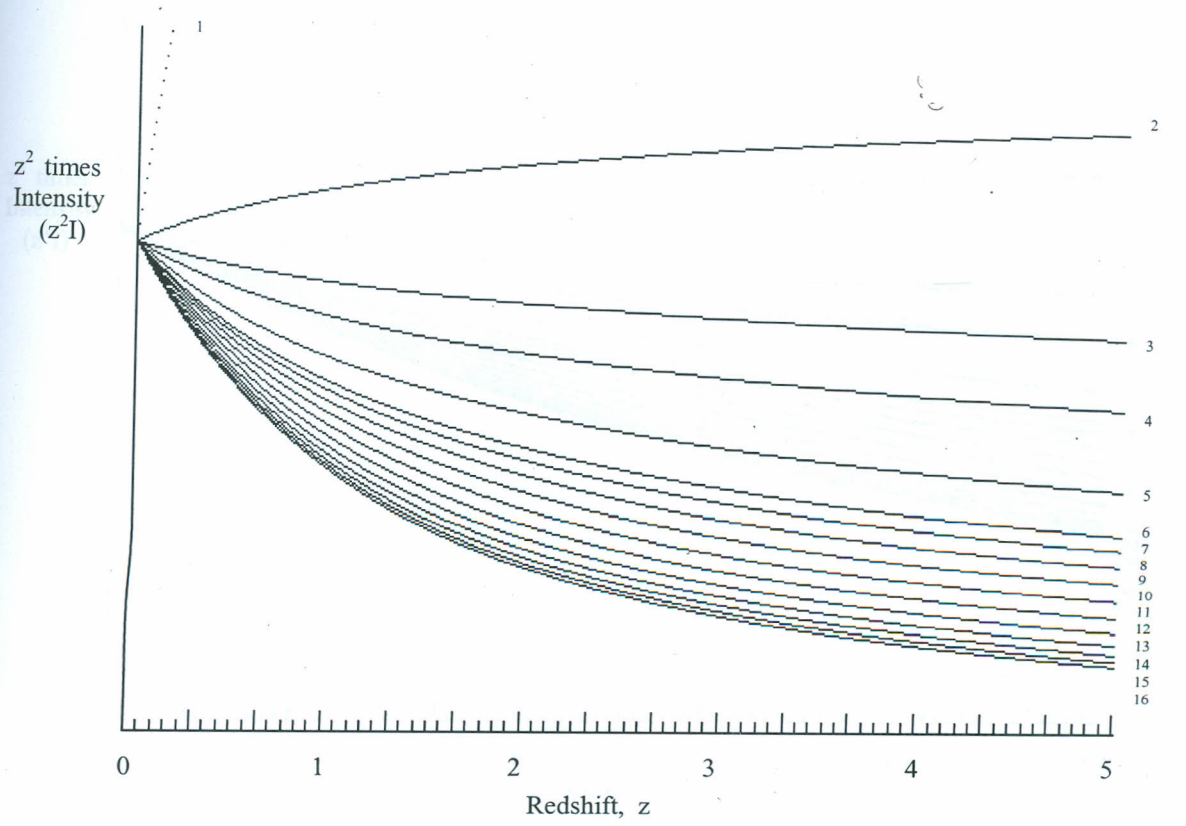

Table of contents for the above figure:- $R(t_o)=9x10^{25}$; steps =10; $\rho_{min}=5x10^{-27}$ and $\rho_{max}=3x10^{-25}$.

Label of curve	Value of ρ	Value of κ
1	8.78E-26	1
2	1.32E-25	
3	1.99E-25	
4	3.00E-25	
5	All curves in the range 5.00E-27 to 3.00E-25 coincide on curve 5	0
6	3.00E-25	-1
7	1.99E-25	
8	1.32E-25	
9	8.78E-26	
10	5.83E-26	
11	3.87E-26	
12	2.57E-26	
13	1.71E-26	
14	1.13E-26	
15	7.53E-27	
16	5.00E-27	

Note:

$$I=L(1+\kappa r(z)^2)^2/((1+z)^2 4\pi r(z)^2 R(t_o)^2)$$

Figure 2:- z^2 times Intensity versus Redshift

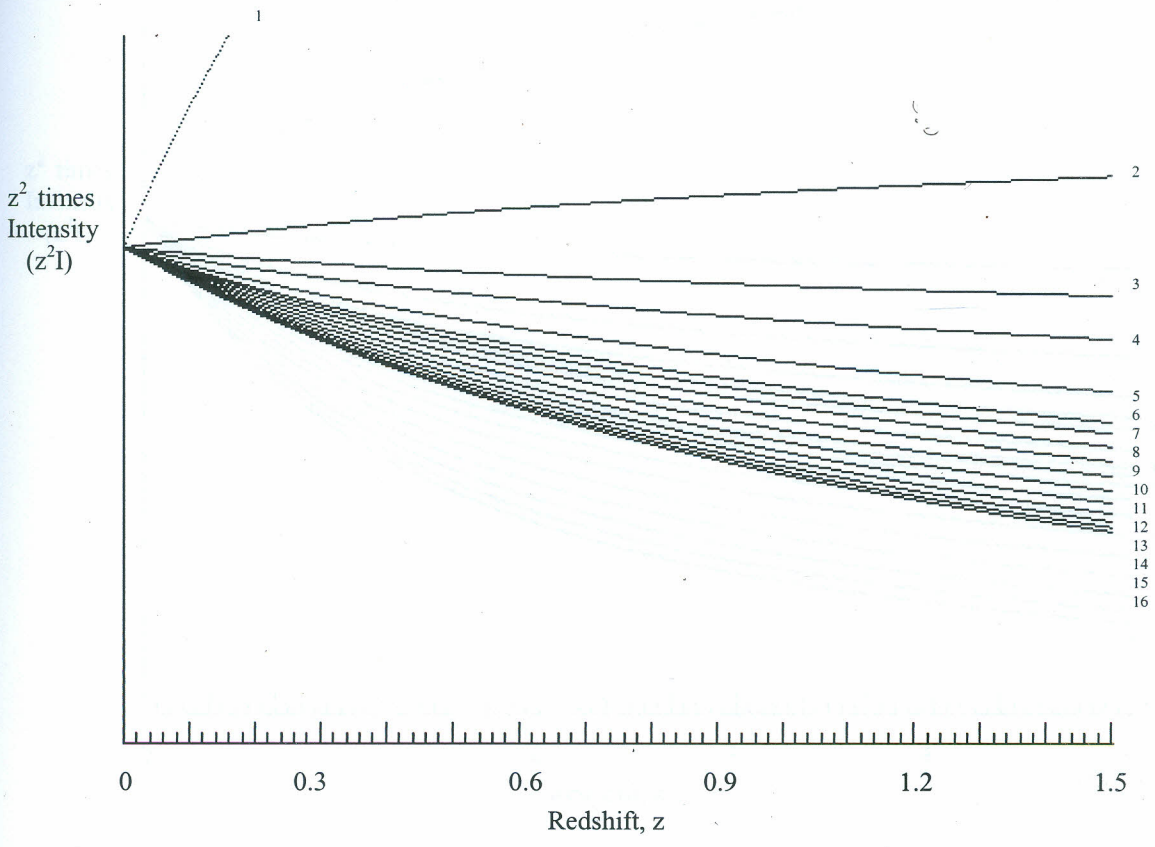

Table of contents for the above figure:- $R(t_o)=9x10^{25}$; steps =10;
$\rho_{min}=5x10^{-27}$ and $\rho_{max}=3x10^{-25}$.

Label of curve	Value of ρ	Value of κ
1	8.78E-26	1
2	1.32E-25	
3	1.99E-25	
4	3.00E-25	
5	All curves in the range 5.00E-27 to 3.00E-25 coincide on curve 5	0
6	3.00E-25	-1
7	1.99E-25	
8	1.32E-25	
9	8.78E-26	
10	5.83E-26	
11	3.87E-26	
12	2.57E-26	
13	1.71E-26	
14	1.13E-26	
15	7.53E-27	
16	5.00E-27	

Note:

$$I=L(1+\kappa r(z)^2)^2/((1+z)^2 4\pi r(z)^2 R(t_o)^2)$$

Figure 3:- z^2 times Intensity versus Redshift

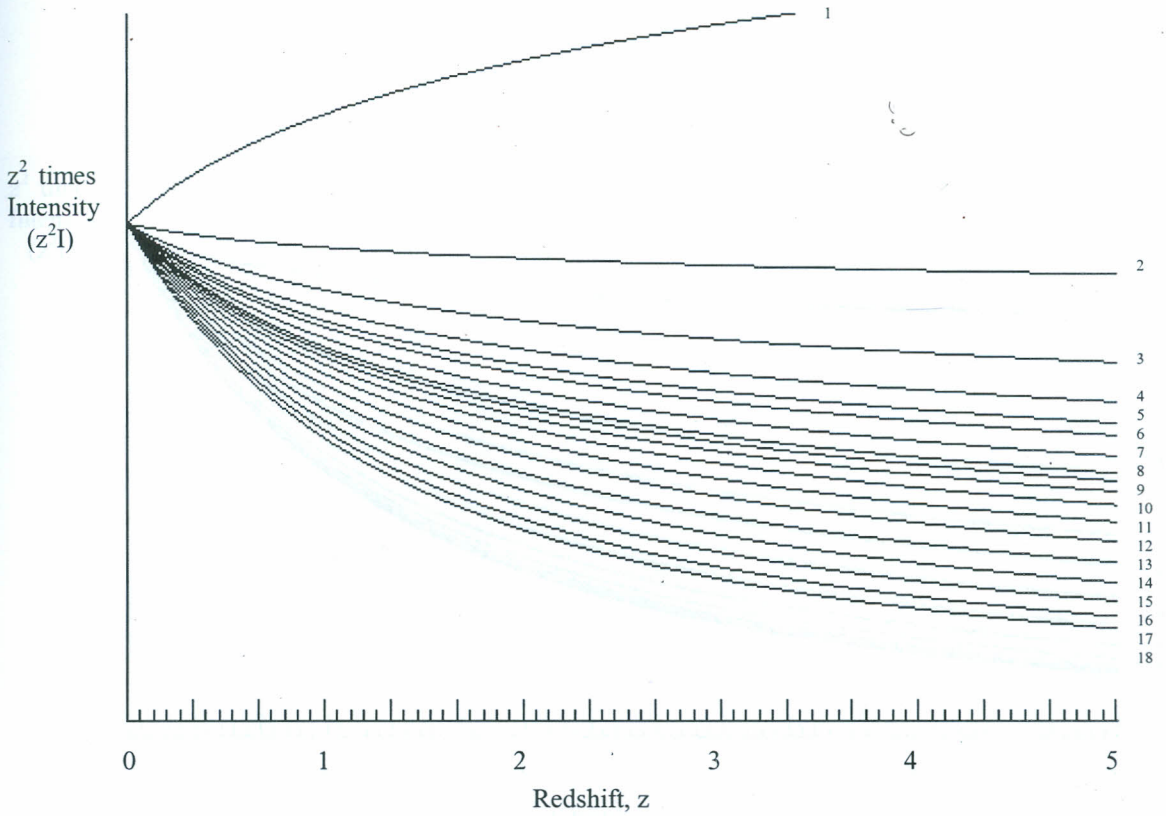

Table of contents for the above figure:- $R(t_o)=5x10^{25}$; steps =10; $\rho_{min}=5x10^{-26}$ and $\rho_{max}=3x10^{-24}$.

Label of curve	Value of ρ	Value of κ
1	3.87E-25	1
2	5.83E-25	
3	8.78E-25	
4	1.32E-24	
5	1.99E-24	
6	1.99E-24	
7	All curves in the range 5.00E-26 to 3.00E-24coincide on curve 7	0
8	3.00 E-24	-1
9	1.99E-24	
10	1.32E-24	
11	8.78E-25	
12	5.83E-25	
13	3.87E-25	
14	2.57E-25	
15	1.71E-25	
16	1.13E-25	
17	7.53E-26	
18	5.00E-26	

Note:

$$I=L(1+\kappa r(z)^2)^2/((1+z)^2 4\pi r(z)^2 R(t_o)^2)$$

Figure 4:- z^2 times Intensity versus Redshift

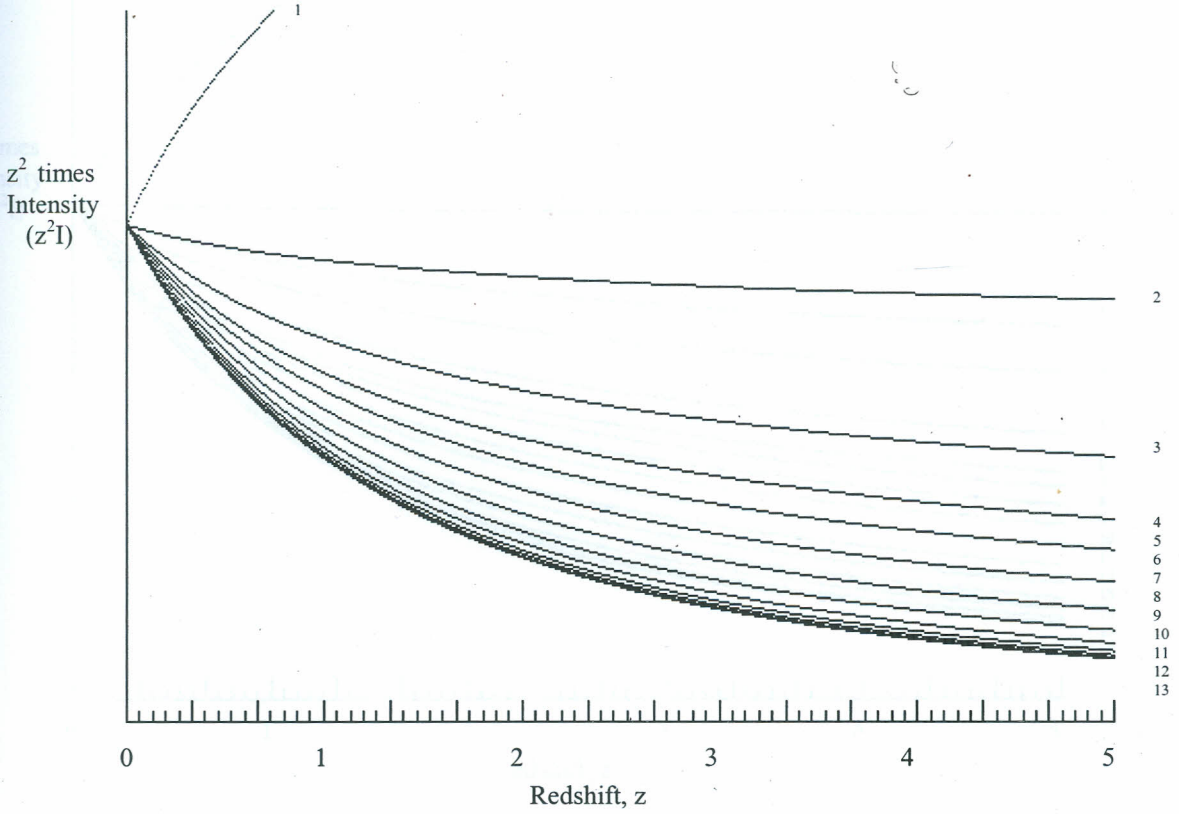

Table of contents for the above figure:- $R(t_o)=1x10^{25}$; steps =10; $\rho_{min}=5x10^{-26}$ and $\rho_{max}=3x10^{-23}$.

Label of curve	Value of ρ	Value of κ
1	8.35E-24	1
2	1.58E-23	
3	All curves in the range 5.00E-26 to 3.00E-23 coincide on curve 3	0
4	1.58E-23	-1
5	8.35E-24	
6	4.40E-24	
7	2.32E-24	
8	1.22E-24	
9	6.46E-25	
10	3.41E-25	
11	1.80E-25	
12	9.48E-26	
13	5.00E-26	

Note:

$$I=L(1+\kappa r(z)^2)^2/((1+z)^2 4\pi r(z)^2 R(t_o)^2)$$

Figure 5:- z^2 times Intensity versus Redshift

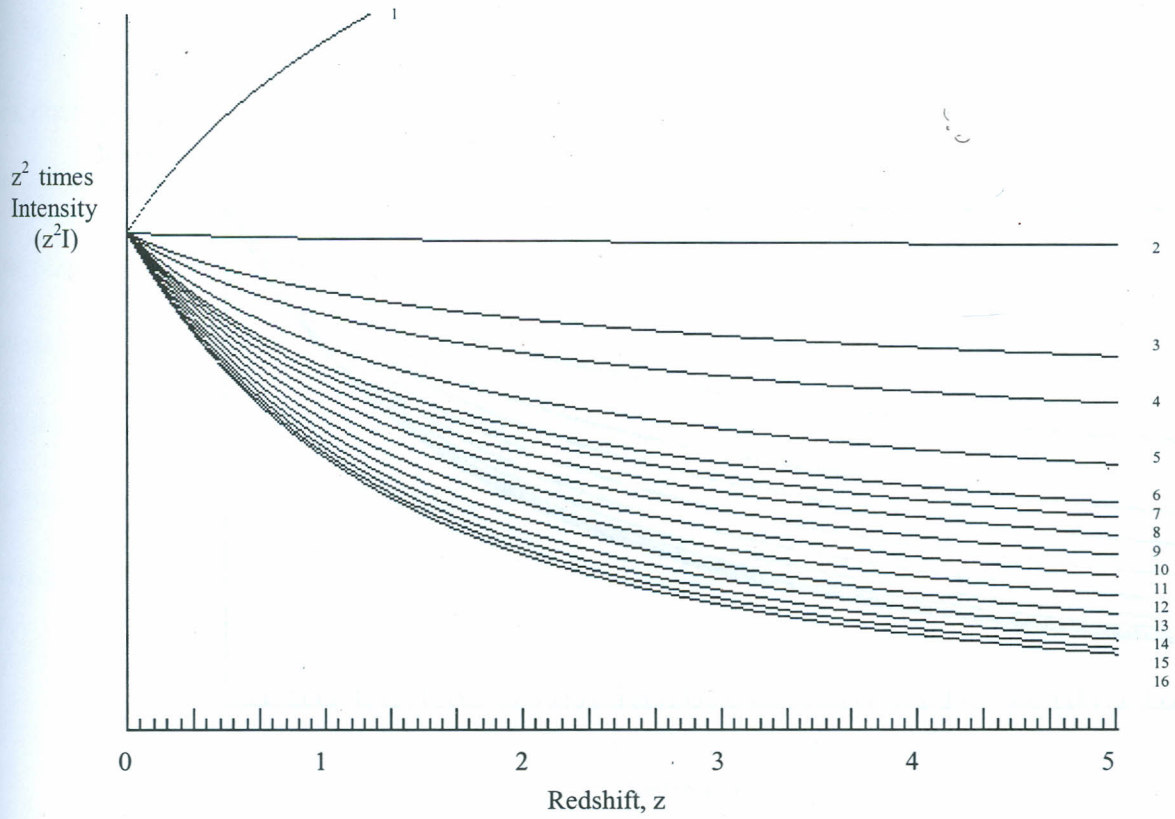

Table of contents for the above figure:- $R(t_o)=1x10^{26}$; steps =10; $\rho_{min}=5x10^{-27}$ and $\rho_{max}=3x10^{-25}$.

Label of curve	Value of ρ	Value of κ
1	8.78E-26	1
2	1.32E-25	
3	1.99E-25	
4	3.00E-25	
5	All curves in the range 5.00E-27 to 3.00E-25 coincide on curve 5	0
6	3.00E-25	-1
7	1.99E-25	
8	1.32E-25	
9	8.78E-26	
10	5.83E-26	
11	3.87E-26	
12	2.57E-26	
13	1.71E-26	
14	1.13E-26	
15	7.53E-27	
16	5.00E-27	

Note:

$$I=L(1+\kappa\, r(z)^2)^2/((1+z)^2 4\pi\, r(z)^2 R(t_o)^2)$$

Figure 6:- z^2 times Intensity versus Redshift

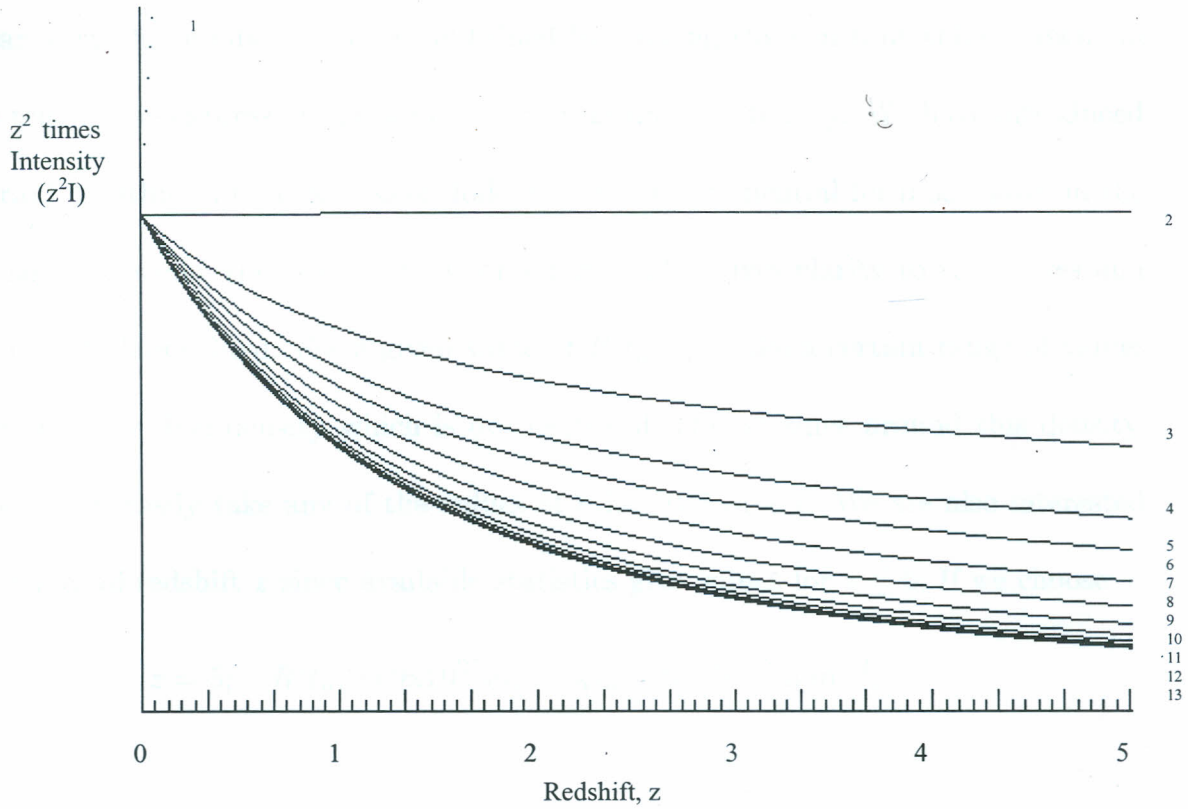

Table of contents for the above figure:- $R(t_o)=9x10^{24}$; steps =10; $\rho_{min}=5x10^{-26}$ and $\rho_{max}=3x10^{-23}$.

Label of curve	Value of ρ	Value of κ
1	8.35E-24	1
2	1.58E-23	
3	All curves in the range 5.00E-26 to 3.00E-23 coincide on curve 3	0
4	1.58E-23	-1
5	8.35E-24	
6	4.40E-24	
7	2.32E-24	
8	1.22E-24	
9	6.46E-25	
10	3.41E-25	
11	1.80E-25	
12	9.48E-26	
13	5.00E-26	

Note:

$$I=L(1+\kappa r(z)^2)^2/((1+z)^2 4\pi r(z)^2 R(t_o)^2)$$

We can vary the number of curves obtained by varying the constant value shown (in this case ten) in the expression for step in our program for intensity. We have introduced the natural logarithm in this expression followed by the exponential form as shown in the program so as to widen the spacing between curves. This gives clarity to the curves and makes it easy to label them. For a given value of $R(t_o)$, we take a certain range of values of ρ around the critical density which is our centre of interest since around this density, the universe can easily take any of the values of κ i.e., $0, 1$ or -1. We are also interested in small values of redshift z since available statistics give values for $z \leq 5$. If we choose

$$z = 5; \quad R(t_o) = 9\text{x}10^{25}\text{m}; \quad \rho_{\text{min}} = 5\text{x}10^{-27}\text{kgm}^{-3};$$

and

$$\rho_{\text{max}} = 3\text{x}10^{-25}\text{kgm}^{-3};$$

while we put the number of steps in our program to be ten, we get the result as shown in figure 1. The same program when run as above but for $z \leq 1.5$ gives the result in figure 2. In figure 1, the curves corresponding to the flat universe $\kappa = 0$ (in this case all curves in the given defined range of ρ from $\rho_{\text{min}} = 5\text{x}10^{-27}\text{kgm}^{-3}$ to $\rho_{\text{max}} = 3\text{x}10^{-25}\text{kgm}^{-3}$) have the label 5 and they separate the open universe ($\kappa = -1$) from the closed universe ($\kappa = 1$). There are only four curves that are possible for the closed universe (labeled 1-4) and eleven ones for the open universe (labeled 6-16). Curves in the closed universe start off very fast, hence $z^2 I$ starts by growing very fast as compared to the open universe as shown in figure 1. In this case, we see that the closed universe (closed curvature) deviates much more from the classical results (flat universe) than the open universe. The case of positive curvature describes a closed universe, whose three- dimensional space is analogous to the surface of a sphere. As the coordinate ranges from zero to one, the r-sphere sweep out the

entire universe leaving it unbounded just as there is no edge encountered on the surface of a sphere. As we decrease the redshift from 5 to 1.5 as shown in figure 2, the deviations of the open and closed universes from the classical results also decrease with the result that curves for the open universe start off roughly as straight lines and get only slightly bent as z increases. This result agrees with the classical expectation. This implies that as $z \to 0$, the deviations from the classical results also tends to zero. This shows that as $z \to 0$, space-time becomes less and less curved so that it is almost flat. This is the observation we would make at the start of the universe since $z \to 0$ implies going backwards in time. It should also be noted that the faster initial growth of $z^2 I$ in the closed universe ($\kappa = 1$) is followed by a faster decrease of $z^2 I$ again as compared to the open universe ($\kappa = -1$). For easy identification and assignment of densities to the curves, the program can be modified by omitting the braces in the main program so that each curve is drawn at a time with its corresponding value of density shown.

Figure 3 results when we vary $R(t_o)$ from $9\text{x}10^{25}$m to $5\text{x}10^{25}$m and give ρ_{min} as $5\text{x}10^{-26}\text{kgm}^{-3}$ while ρ_{max} as $3\text{x}10^{-24}\text{kgm}^{-3}$ in our program. In this case there are six curves for the closed universe (labeled 1-6) and eleven curves for the open universe. Sandwiched between the open and the closed universes are all curves in this given range of ρ corresponding to the flat universe. Unlike in figures 1 and 2, both the open and closed universes here start off growing slowly, hence $z^2 I$ increases slowly and, as z increases, the deviations from the classical results also increase but faster for $\kappa = 1$ than for $\kappa = -1$. $z^2 I$ increases faster in a closed universe than in an open universe. So in a closed universe, the intensity would generally decrease at a faster rate as the r-spheres sweep out the entire universe than in an open universe. This result is in agreement with the Friedmann

cosmology of a closed universe.

If we now reduce $R(t_o)$ from $5\text{x}10^{25}$m to $1\text{x}10^{25}$m, and $\rho_{\max}$ from $3\text{x}10^{-23}\text{kgm}^{-3}$ to $3\text{x}10^{-24}\text{kgm}^{-3}$, we get the results as shown in figure 4. In this case there are only two possible curves for the universe corresponding to $\kappa = 1$. The curves corresponding to the flat universe ($\kappa = 0$) in the above given range of ρ are denoted by label 3. The curves in this case for the closed universe start off at a faster rate than for the open universe.

Let us now fix the range of ρ, the number of steps, and the redshift z as in figure 1 but increase $R(t_o)$ from $9\text{x}10^{25}$m to $1\text{x}10^{26}$m. If we do this, we get the results as shown in figure 5. We note that increasing $R(t_o)$ in this case results in a similar number of curves but of different shapes. In figure 1, curves for $\kappa = 1$ start off at a faster growth rate than for the same value of κ as shown in figure 5. Reducing the radius is analogous to a compressed gas that would suddenly expand on release. Therefore, reduced radius implies fast expansion of the universe. This further implies that, if our universe started off as a 'point-like' form, then it is true that it must have rushed off in expansion as a 'big bang'.

In figure 6, we have the same values of maximum redshift z, range of ρ and number of steps like in figure 4 except that the radius of the universe has been decreased to $9\text{x}10^{24}$m. We note that curves start increasing faster for this reduced radius of the universe as compared to that of figure 4 for the same reason as given above.

2. Number Density of Galaxies versus Redshift

We now write the program (named galaxy as shown in appendix 2) to investigate the relationship between the number density of galaxies per unit redshift interval $n(z)$ against redshift z. We run the program as we did for intensity by varying $R(t_o)$(m) and $\rho(\text{kgm}^{-3})$

except that in this case, for the sake of clarity, we draw separate graphs for each of the three cases of our universe i.e., $\kappa = 0, 1$ or -1 as shown in figures 7-21 below:

Figure 7:- Number Density of Galaxies versus Redshift for $\kappa=0$

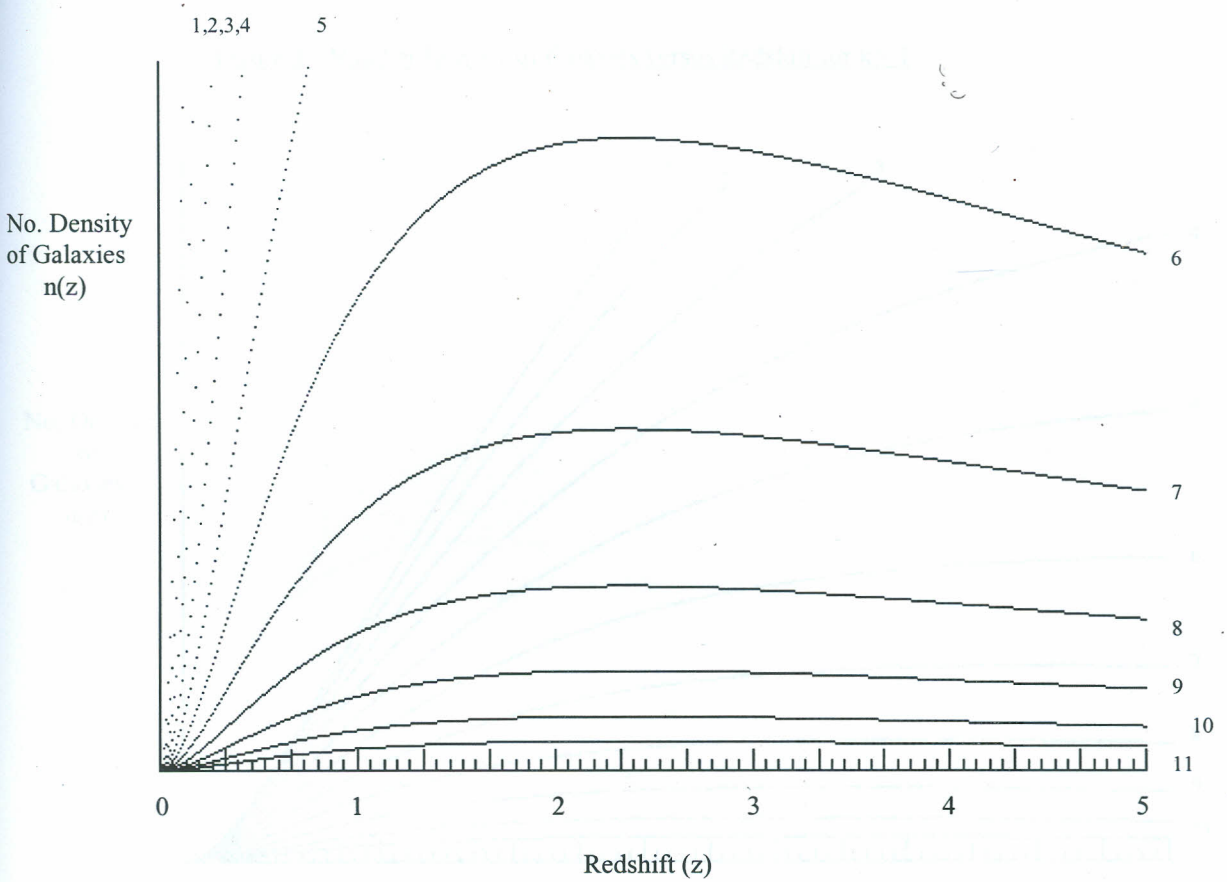

Table of contents for the above figure:- $R(t_o)=9x10^{25}$; steps =10; $\rho_{min}=5x10^{-27}$ and $\rho_{max}=3x10^{-25}$.

Label of curve	Value of ρ
1	5.00E-27
2	7.53E-27
3	1.13E-26
4	1.71E-26
5	2.57E-26
6	3.87E-26
7	5.83E-26
8	8.78E-26
9	1.32E-25
10	1.99E-25
11	3.00E-25

Figure 8:- Number Density of Galaxies versus Redshift for κ=-1

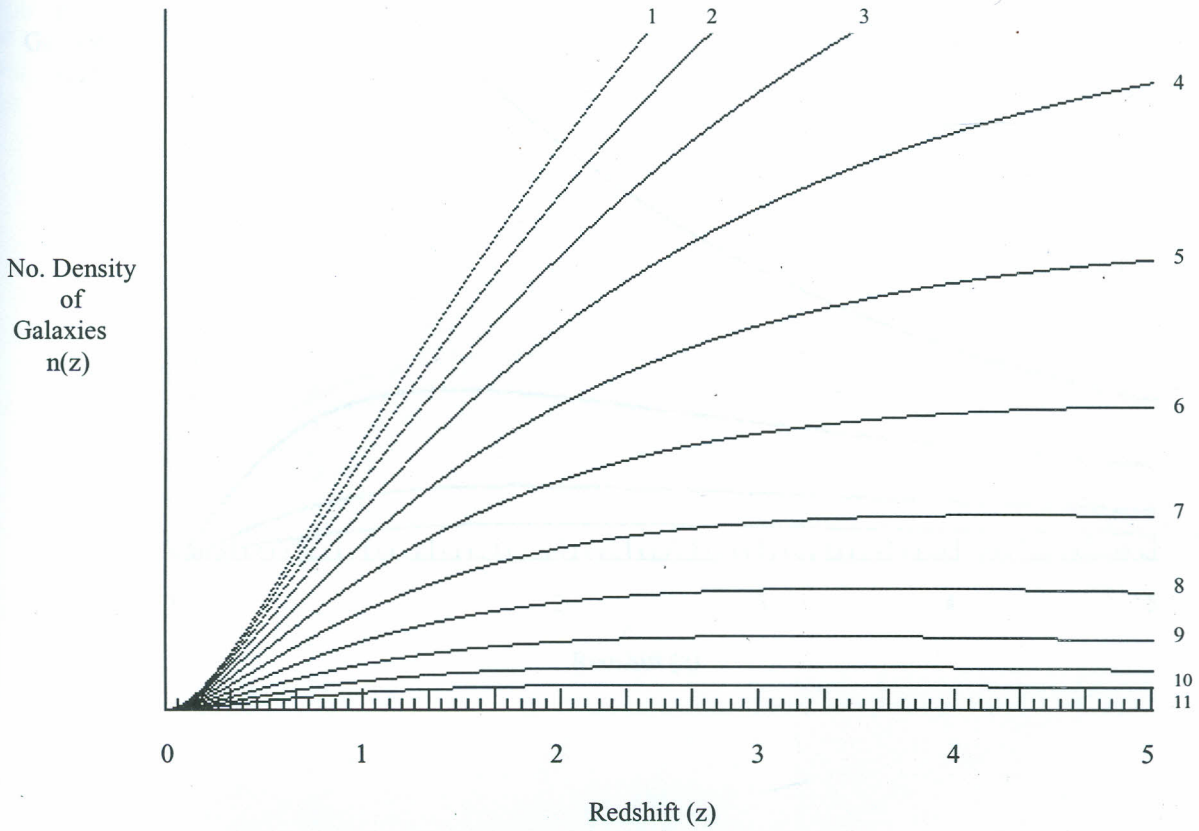

Table of contents for the above figure:- $R(t_o)=9x10^{25}$; steps =10; $\rho_{min}=5x10^{-27}$ and $\rho_{max}=3x10^{-25}$.

Label of curve	Value of ρ
1	5.00E-27
2	7.53E-27
3	1.13E-26
4	1.71E-26
5	2.57E-26
6	3.87E-26
7	5.83E-26
8	8.78E-26
9	1.32E-25
10	1.99E-25
11	3.00E-25

Figure 9:- Number Density of Galaxies versus Redshift for κ=1

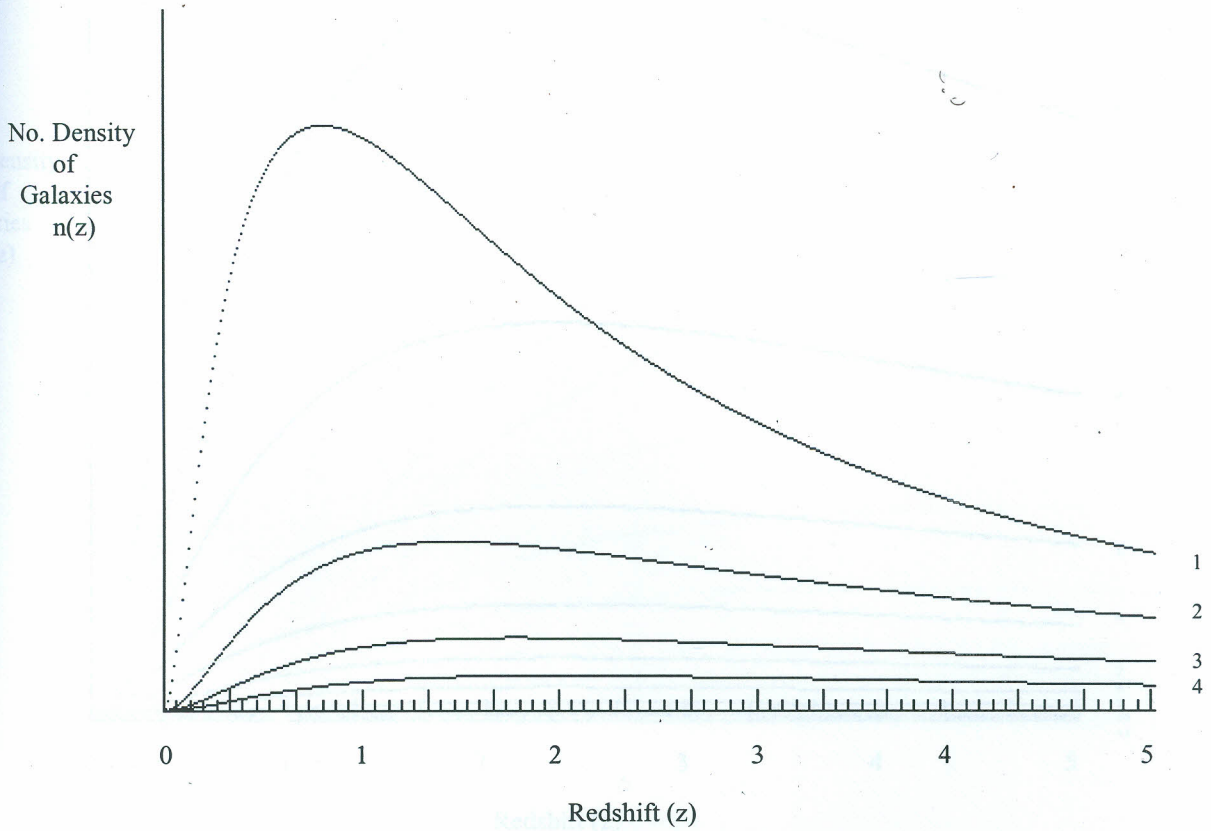

Table of contents for the above figure:- $R(t_o)=9x10^{25}$; steps =10; $\rho_{min}=5x10^{-27}$ and $\rho_{max}=3x10^{-25}$.

Label of curve	Value of ρ
1	8.78E-26
2	1.32E-25
3	1.99E-25
4	3.00E-25

Figure 11:- Number Density of Galaxies versus Redshift for κ=-1

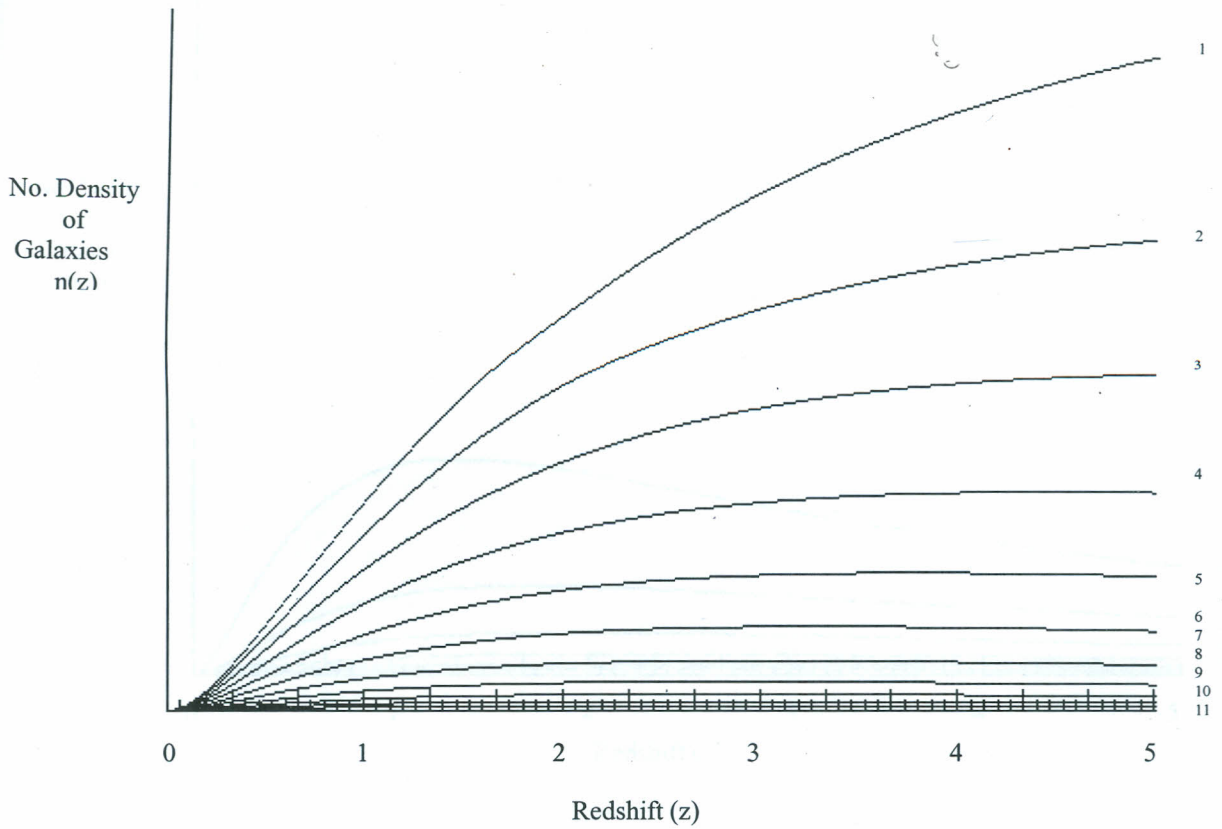

Table of contents for the above figure:- $R(t_o)=5x10^{25}$; steps =10; $\rho_{min}=5x10^{-26}$ and $\rho_{max}=3x10^{-24}$.

Label of curve	Value of ρ
1	5.00E-26
2	7.53E-26
3	1.13E-25
4	1.71E-25
5	2.57E-25
6	3.87E-25
7	5.83E-25
8	8.78E-25
9	1.32E-24
10	1.99E-24
11	3.00E-24

Figure 12:- Number Density of Galaxies versus Redshift for $\kappa=1$

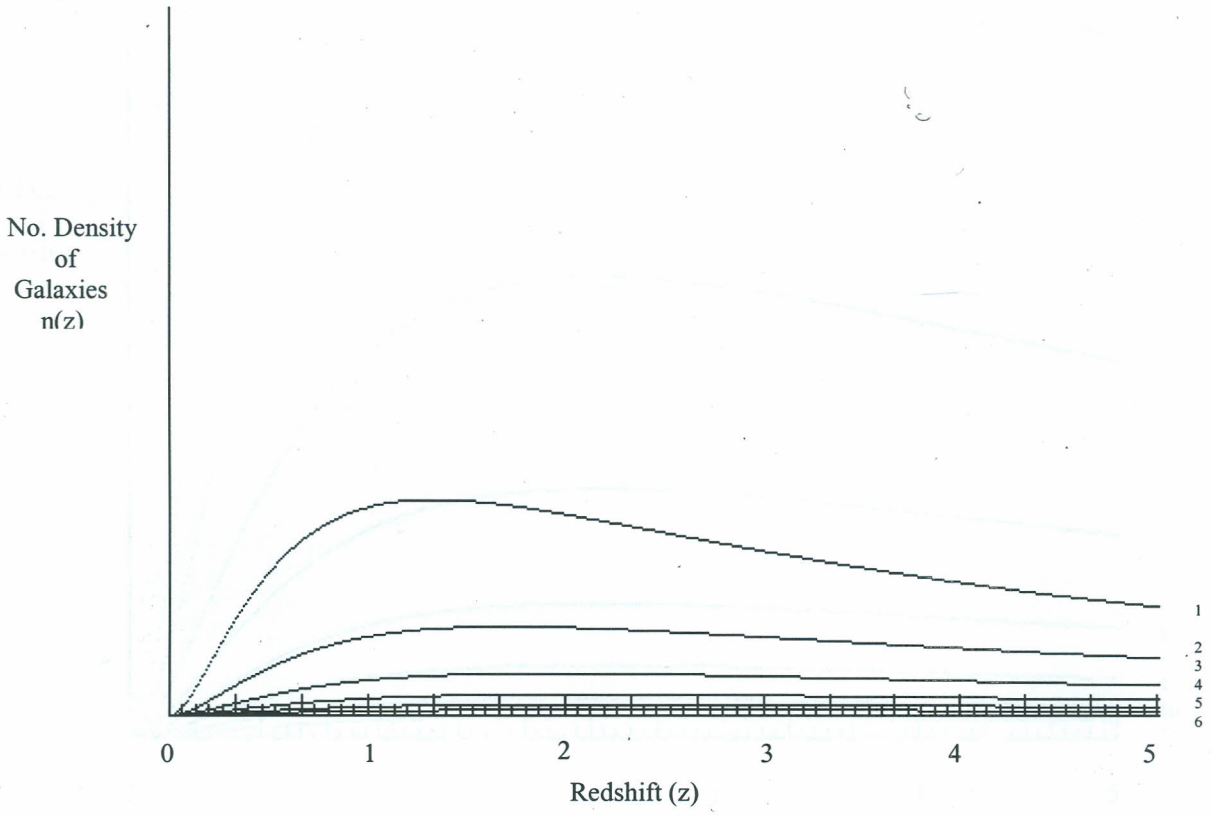

Table of contents for the above figure:- $R(t_o)=5x10^{25}$; steps =10; $\rho_{min}=5x10^{-26}$ and $\rho_{max}=3x10^{-24}$.

Label of curve	Value of ρ
1	3.87E-25
2	5.83E-25
3	8.78E-25
4	1.32E-24
5	1.99E-24
6	3.00E-24

Figure 13:- Number Density of Galaxies versus Redshift for κ=0

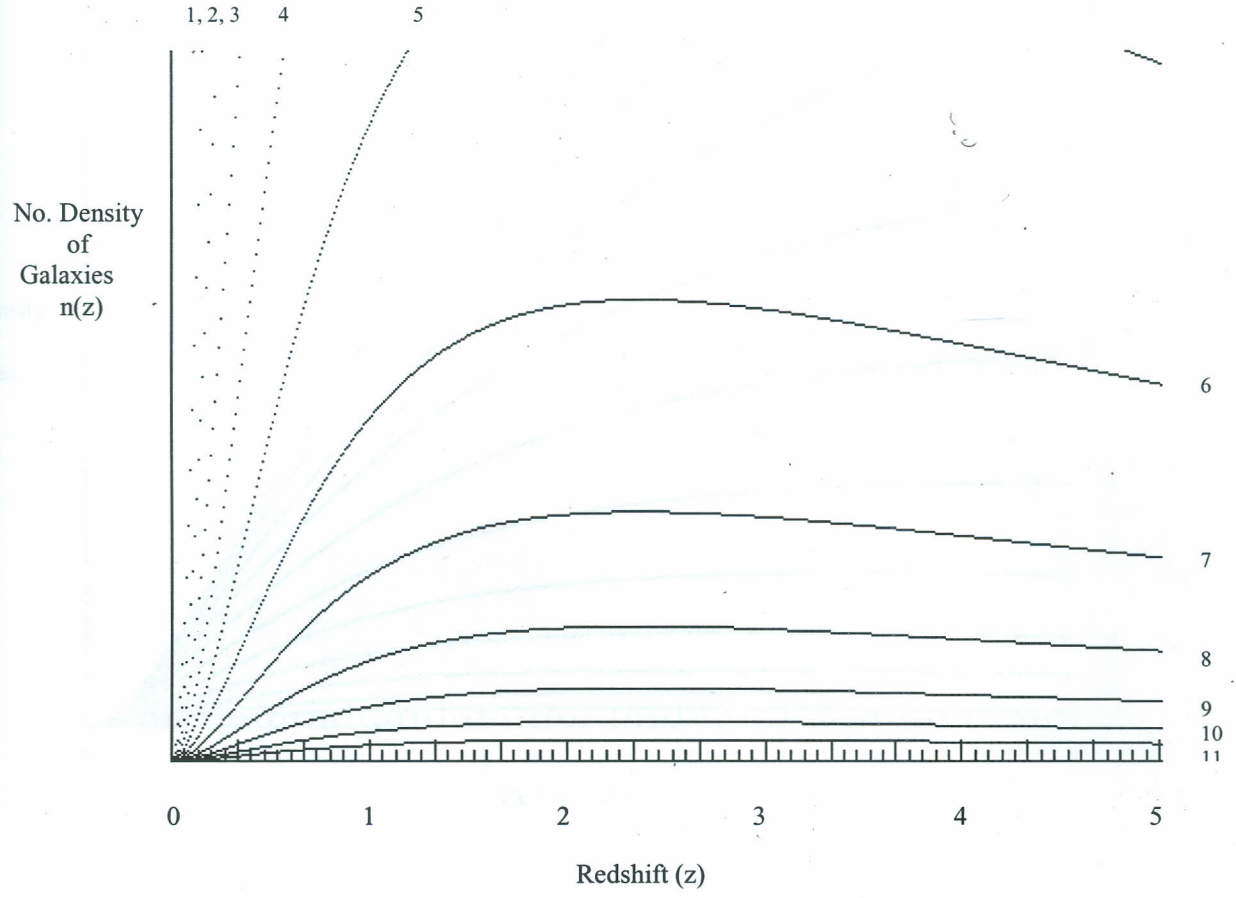

Table of contents for the above figure:- $R(t_o)=1x10^{25}$; steps =10; $\rho_{min}=5x10^{-25}$ and $\rho_{max}=3x10^{-23}$.

Label of curve	Value of ρ
1	5.00E-25
2	7.53E-25
3	1.13E-24
4	1.71E-24
5	2.57E-24
6	3.87E-24
7	5.83E-24
8	8.78E-24
9	1.32E-23
10	1.99E-23
11	3.00E-23

Figure 14:- Number Density of Galaxies versus Redshift for κ=-1

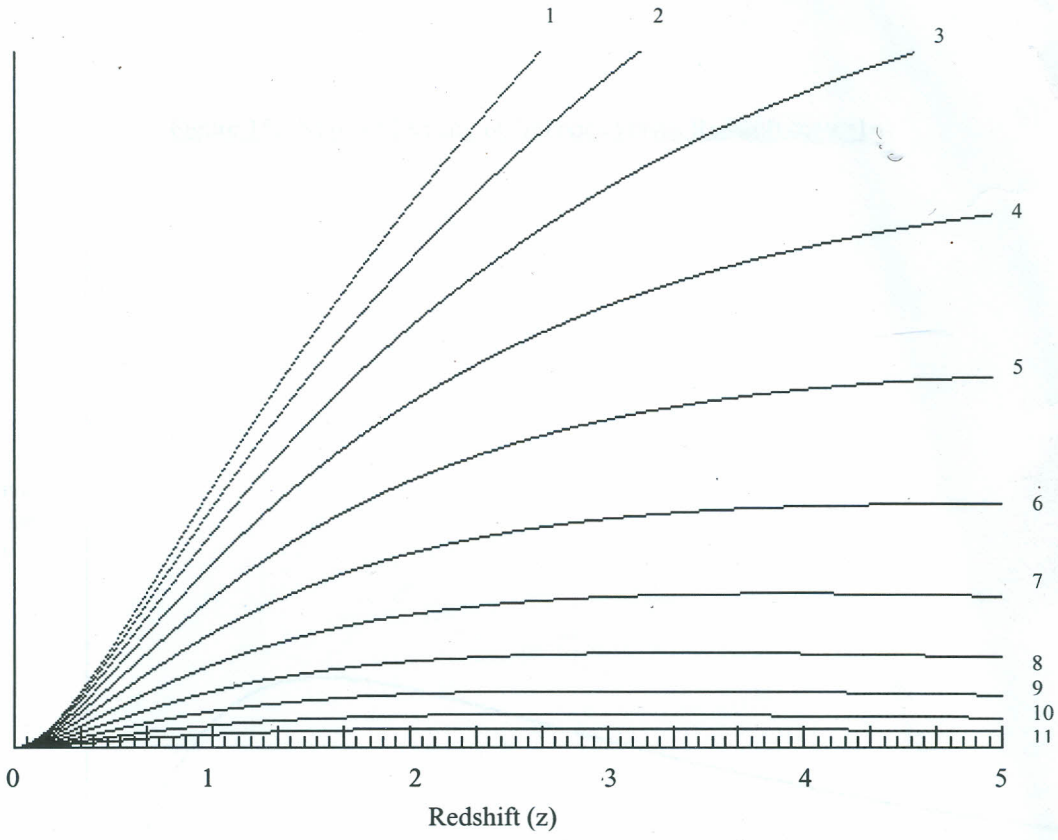

Table of contents for the above figure:- $R(t_o)=1x10^{25}$; steps =10; $\rho_{min}=5x10^{-25}$ and $\rho_{max}=3x10^{-23}$.

Label of curve	Value of ρ
1	5.00E-25
2	7.53E-25
3	1.13E-24
4	1.71E-24
5	2.57E-24
6	3.87E-24
7	5.83E-24
8	8.78E-24
9	1.32E-23
10	1.99E-23
11	3.00E-23

Figure 15:- Number Density of Galaxies versus Redshift for $\kappa=1$

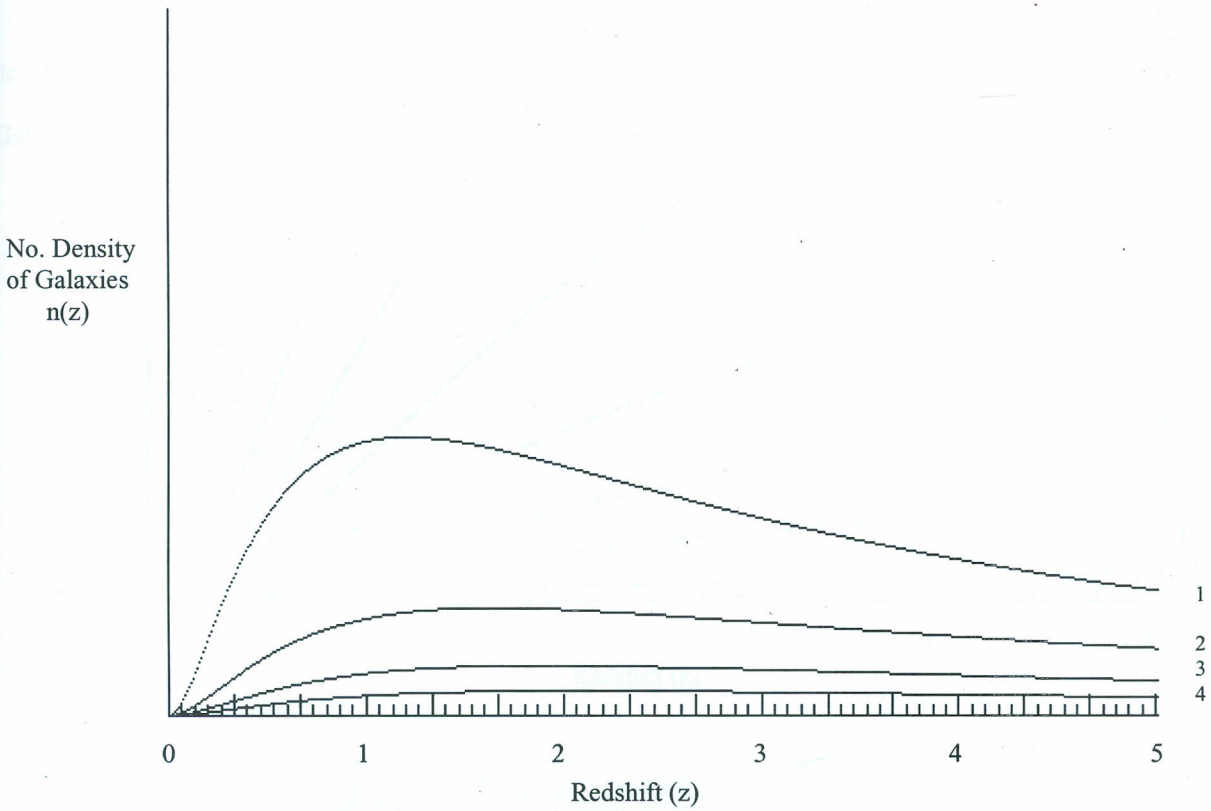

Table of contents for the above figure:- $R(t_o)=1x10^{25}$; steps =10;
$\rho_{min}=5x10^{-25}$ and $\rho_{max}=3x10^{-23}$.

Label of curve	Value of ρ
1	8.78E-24
2	1.32E-23
3	1.99E-23
4	3.00E-23

Figure 16:- Number Density of Galaxies versus Redshift for $\kappa=0$

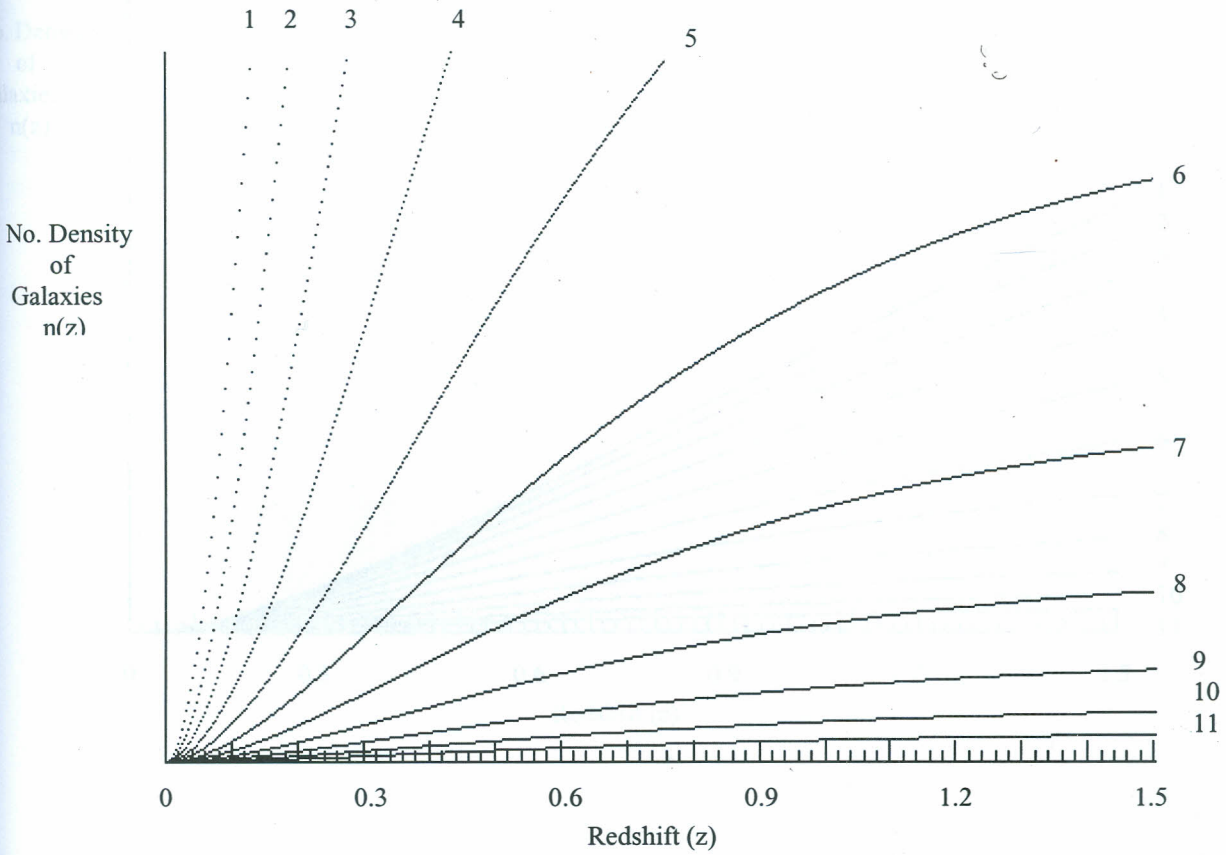

Table of contents for the above figure:- $R(t_o)=9x10^{25}$; steps =10; $\rho_{min}=5x10^{-27}$ and $\rho_{max}=3x10^{-25}$.

Label of curve	Value of ρ
1	5.00E-27
2	7.53E-27
3	1.13E-26
4	1.71E-26
5	2.57E-26
6	3.87E-26
7	5.83E-26
8	8.78E-26
9	1.32E-25
10	1.99E-25
11	3.00E-25

Figure 17:- Number Density of Galaxies versus Redshift for $\kappa = -1$

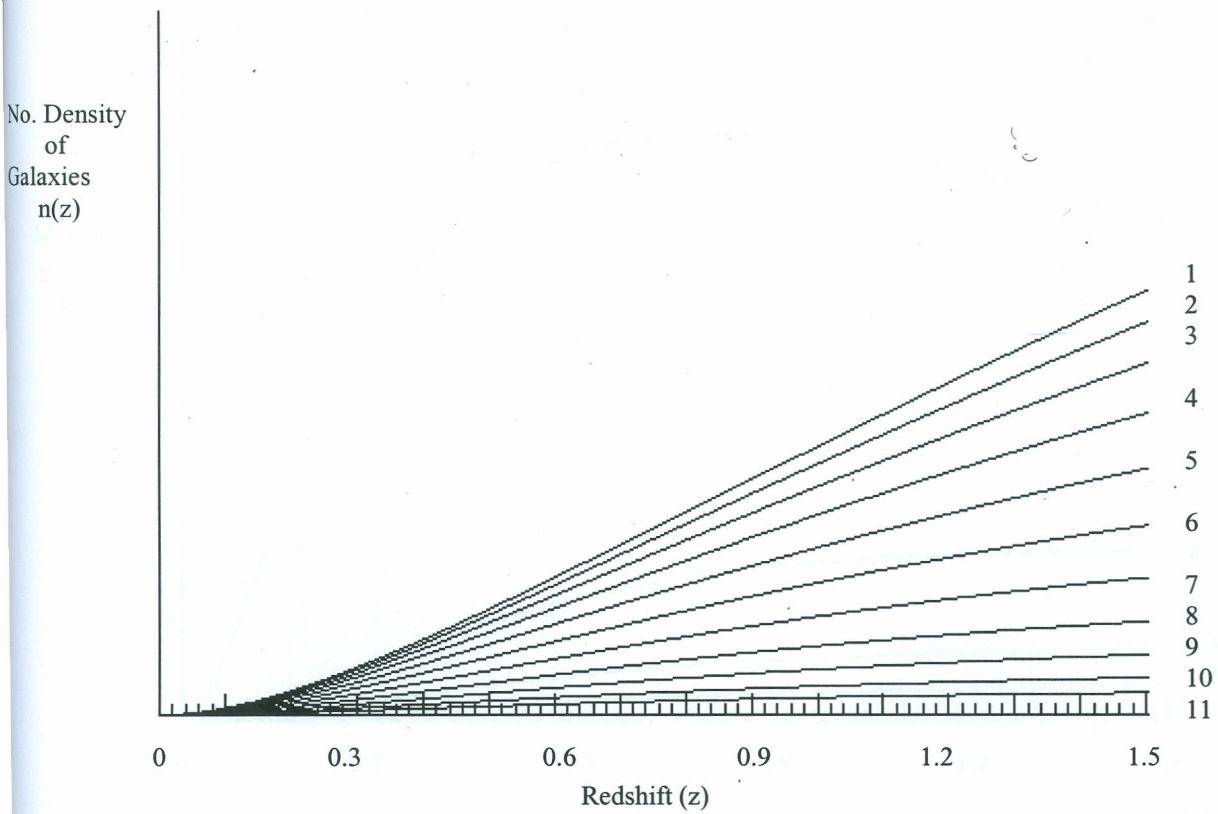

Table of contents for the above figure:- $R(t_o)=9\times10^{25}$; steps =10; $\rho_{min}=5\times10^{-27}$ and $\rho_{max}=3\times10^{-25}$.

Label of curve	Value of ρ
1	5.00E-27
2	7.53E-27
3	1.13E-26
4	1.71E-26
5	2.57E-26
6	3.87E-26
7	5.83E-26
8	8.78E-26
9	1.32E-25
10	1.99E-25
11	3.00E-25

Figure 18:- Number of galaxies versus Redshift for $\kappa=1$

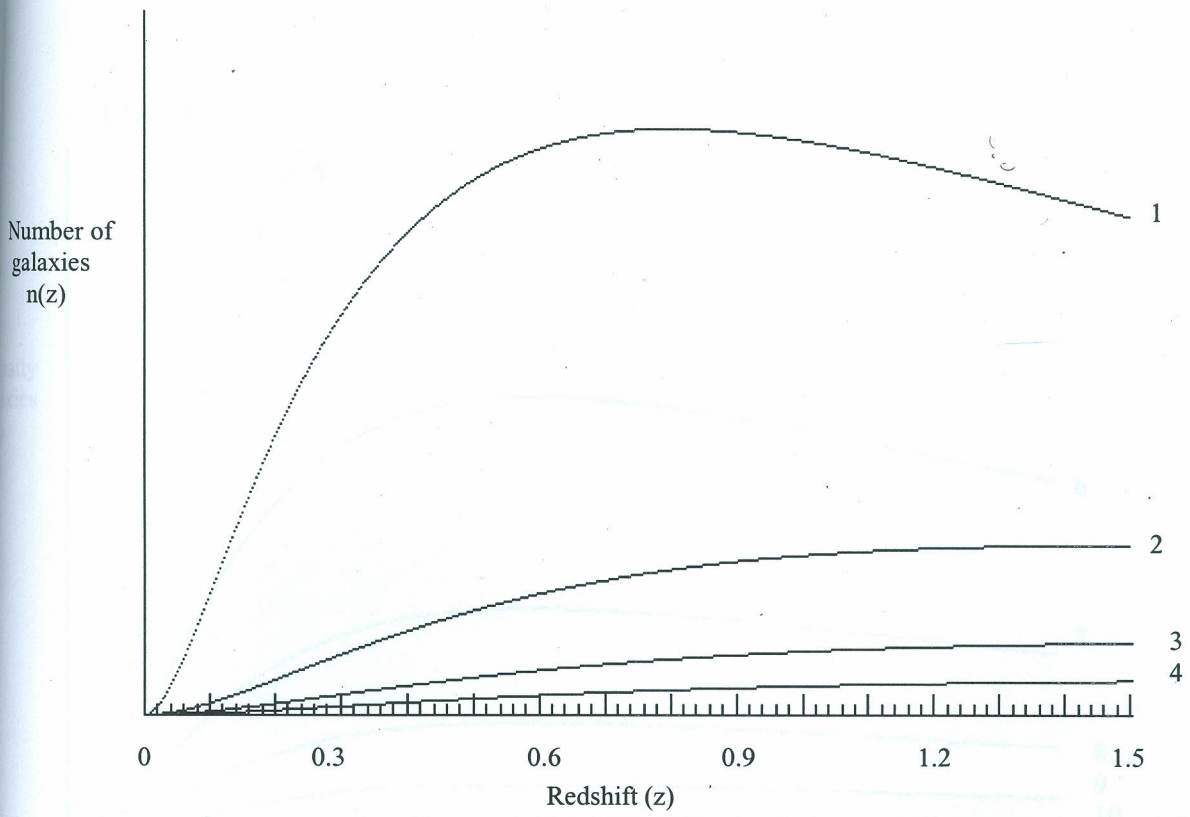

Table of contents for the above figure:- $R(t_o)=9x10^{25}$; steps =10; $\rho_{min}=5x10^{-27}$ and $\rho_{max}=3x10^{-25}$.

Label of curve	Value of ρ
1	8.78E-26
2	1.32E-25
3	1.99E-25
4	3.00E-25

Figure 19:- Number Density of Galaxies versus Redshift for κ=0

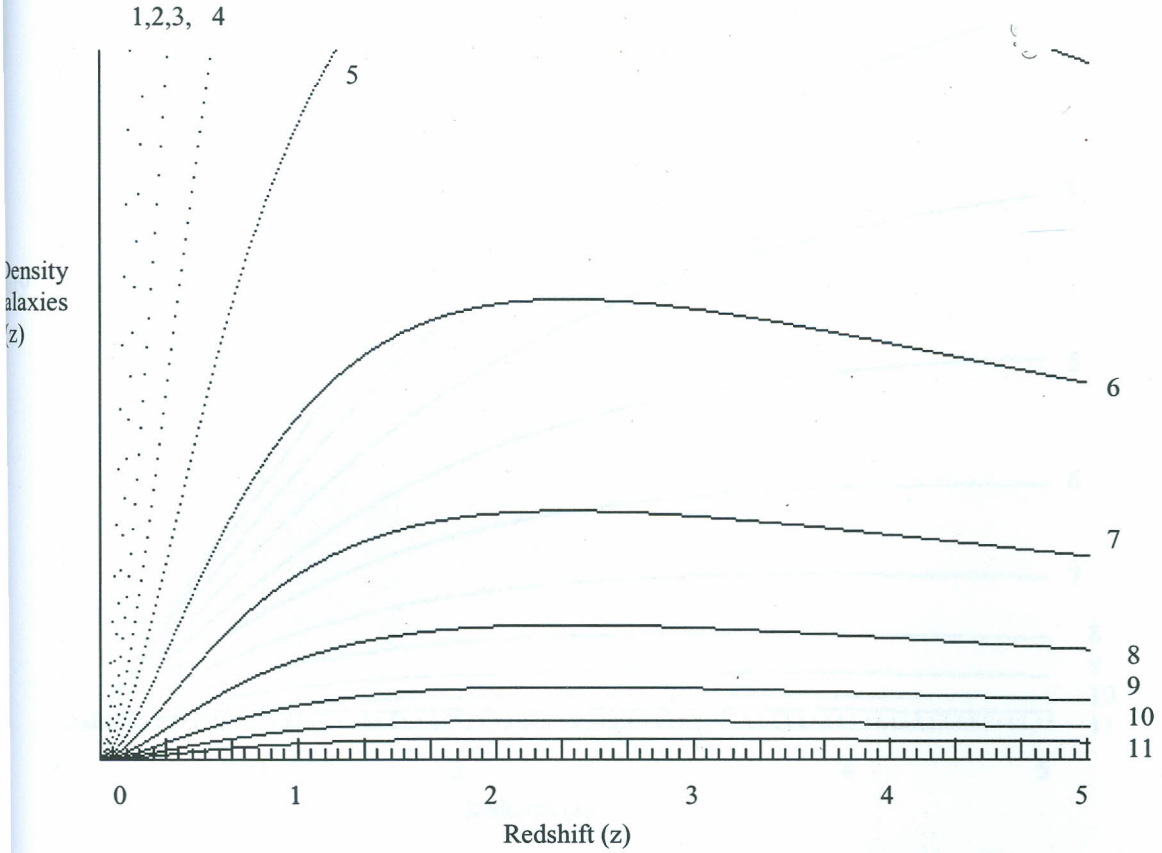

Table of contents for the above figure:- $R(t_o)=1x10^{26}$; steps =10; $\rho_{min}=5x10^{-27}$ and $\rho_{max}=3x10^{-25}$.

Label of curve	Value of ρ
1	5.00E-27
2	7.53E-27
3	1.13E-26
4	1.71E-26
5	2.57E-26
6	3.87E-26
7	5.83E-26
8	8.78E-26
9	1.32E-25
10	1.99E-25
11	3.00E-25

Figure 20:- Number Density of Galaxies versus Redshift for κ= -1

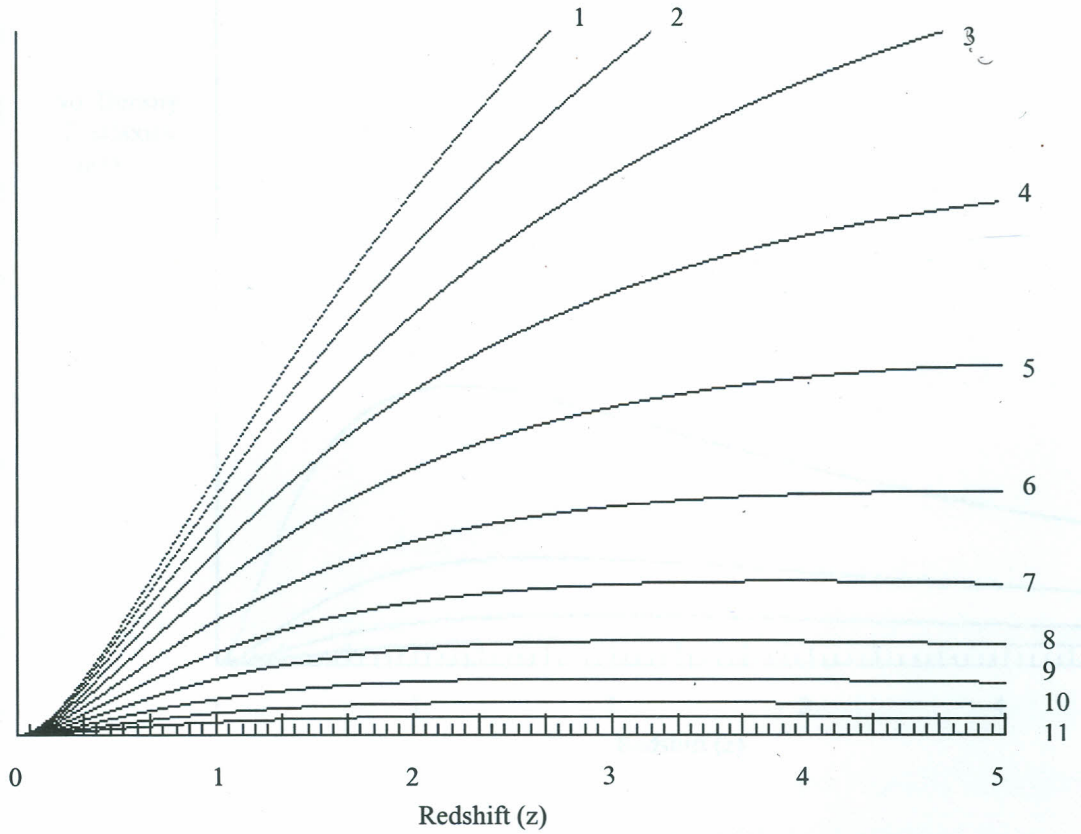

Table of contents for the above figure:- $R(t_o)=1x10^{26}$; steps =10; $\rho_{min}=5x10^{-27}$ and $\rho_{max}=3x10^{-25}$.

Label of curve	Value of ρ
1	5.00E-27
2	7.53E-27
3	1.13E-26
4	1.71E-26
5	2.57E-26
6	3.87E-26
7	5.83E-26
8	8.78E-26
9	1.32E-25
10	1.99E-25
11	3.00E-25

Figure 21:- Number Density of Galaxies versus Redshift for κ=1

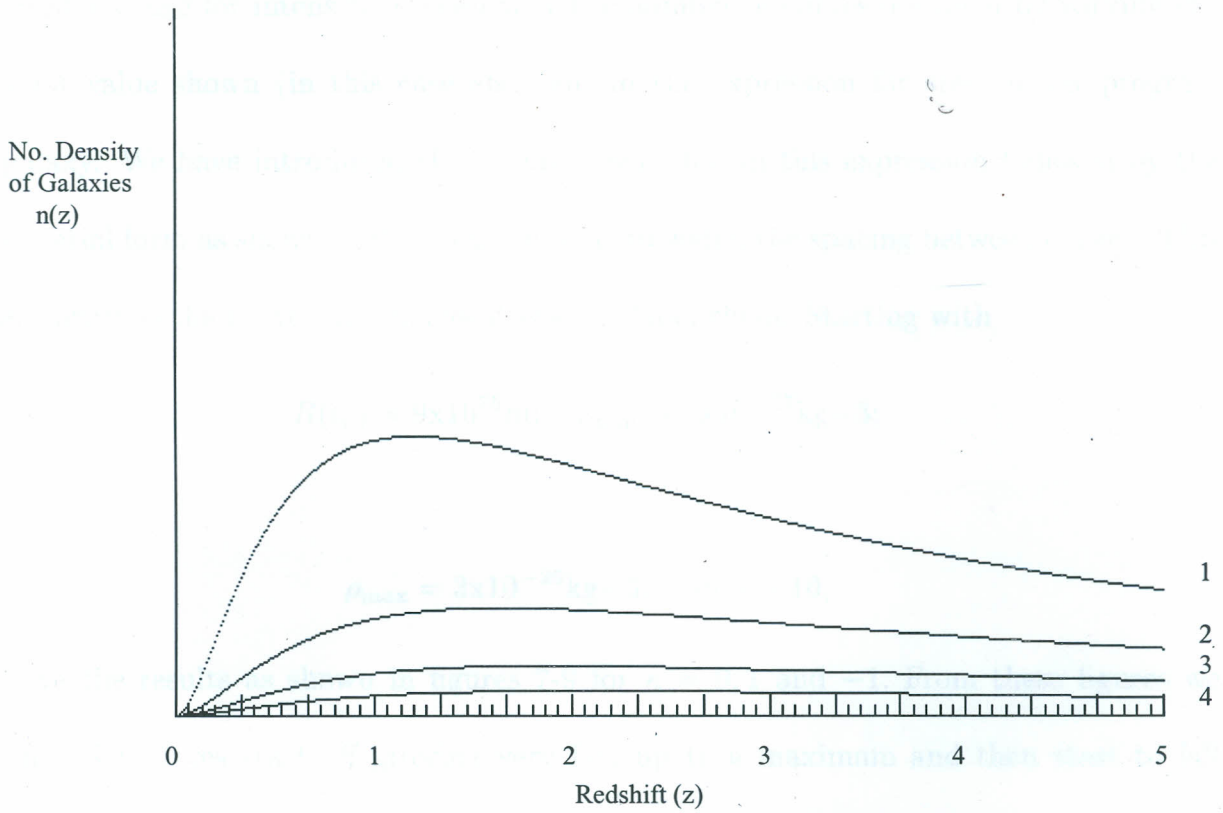

Table of contents for the above figure:- $R(t_o)=1x10^{26}$; steps =10;
$\rho_{min}=5x10^{-27}$ and $\rho_{max}=3x10^{-25}$.

Label of curve	Value of ρ
1	8.78E-26
2	1.32E-25
3	1.99E-25
4	3.00E-25

Similarly, like for intensity, we can vary the number of curves obtained by varying the constant value shown (in this case also ten) in the expression for step in our program for galaxy. We have introduced the natural logarithm in this expression followed by the exponential form as shown in the program so as to widen the spacing between curves. This gives clarity to the curves and makes it easy to label them. Starting with

$$R(t_o) = 9\text{x}10^{25}\text{m}; \quad \rho_{\min} = 5\text{x}10^{-27}\text{kg}-3;$$

while

$$\rho_{\max} = 3\text{x}10^{-25}\text{kg}-3; \quad \text{step} = 10,$$

we have the results as shown in figures 7-9 for $\kappa = 0, 1$ and -1. From these figures we see that the curves start off growing very fast up to a maximum and then start to fall off. This shows that the number density of galaxies per unit redshift interval $n(z)$ start off increasing very fast with increase in redshift up to some maximum value before starting to decrease again. This means that at the beginning of the formation of the universe, $n(z)$ was very low but has increased with time as more and more galaxies have been formed in relation to the rate of expansion of our universe. This observation is in accordance with the structure formation theory for the Friedmann universe. According to this theory, matter is formed to compensate for the expansion. The rate of increase of $n(z)$ in a flat universe is faster than in a closed or open universe. The spacing between curves reduces more gradually with an increase in redshift for a flat universe ($\kappa = 0$) than for a closed universe ($\kappa = 1$). Curves increase less rapidly for the open universe at the start and build up to a smaller peak than for the flat universe and then rapidly falls back as the redshift increases. This shows that the rate of formation of structures i.e., galaxies, is faster in an uncurved universe than in a curved one. For the open universe ($\kappa = -1$), the curves start

off with a greater deviation from the flat universe and reach the peak at a higher value of redshift than for the open and closed universes. There are only four curves to be drawn for the universe corresponding to $\kappa = 1$. These four curves would be the curves to correspond to our universe that is closed.

Let us now assign the following values to the parameters in our program:-

$$R(t_o) = 5\text{x}10^{25}\text{m}; \quad \rho_{\text{min}} = 5\text{x}10^{-26}\text{kg}-3\ ;$$

$$\rho_{\text{max}} = 3\text{x}10^{-24}\text{kg}-3; \quad \text{steps} = 10.$$

If we do this, figures 10-12 result. In this case, $n(z)$ grows less rapidly for this choice of ρ and $R(t_o)$ as compared to the results shown in figures 7-9. As we go down the table of values, we see that the density of the universe increases. Curves corresponding to high densities reach higher maximum values of $n(z)$ at lower redshift values as compared to curves of lower densities even though they have the same values of κ. High densities are therefore associated with high values of $n(z)$. This new choice of $R(t_o)$ and ρ results in a lower maximum peak for all the values of κ.

Further reduction of $R(t_o)$ to $1\text{x}10^{25}$m results in a new critical density with the choice of $\rho_{\text{min}} = 5\text{x}10^{-25}\text{kg}-3$ and $\rho_{\text{max}} = 3\text{x}10^{-23}\text{kg}-3$. The results of the program for this choice of parameters are shown in figures 13-15. We note that the rate of growth of curves is higher in this case than in the above case for figures 10-12. The curves in figures 13-15 reach their peak values at higher values of z than in figures 10-12. The curves corresponding to $\kappa = 1$ grow much more slowly than for the other values of κ. We only get four curves for $\kappa = 1$ in this case. Reduced radius as above results in increased value of density and as seen from above, this is further associated with high values of $n(z)$. The four curves would

be the curves that would correspond to our universe of $\kappa = 1$.

We now consider figures 16-18 . Here, we repeat the choice of parameters as in figures 7-9 with z value only reduced from 5 to 2. Choosing a smaller scale interval and expanding it accordingly in this case reduces all slopes by a constant factor. We do not obtain any new features by expanding the scale interval but we get more detail on the interval on which we may expect more observational data. As shown in the figures, decreased redshift has an overall effect on the shape of the curves. Decreased redshift results in less rapidly increasing curves for all values of κ. As already explained, decreased redshift means going backwards in time when galaxies were few and the universe was starting off the expansion.

Let us now fix all the choice of parameters made in figures 7-9, but increase $R(t_o)$ from $9x10^{25}$ to $1x10^{26}$. Doing this gives rise to figures 19-21. Increased radius of the universe as can be seen from figures 19-21 results in slow rate of growth of the curves and lower peak values as compared to figures 7-9. Increased radius may be associated with increased expansion rate which is faster than formation of galaxies, hence low value of $n(z)$ and that of density.

4.5 How to Fit an Experimental Curve onto a Theoretical Curve

We now give the procedure of fitting an experimental curve onto a theoretical curve as follows: suppose we have obtained the right experimental data that we need to compare with our theoretical predictions, then we can compare the curve from this data with our theoretical curves. We make this comparison for curves with similar scales. If the scale for the experimentally obtained curve is not the same as the scale of our theoretical curves, then we graduate our theoretical scales so that they are the same as the experimental scale. We ensure that we use the same value of maximum redshift z in our scale like the one used in the experimental scale. An efficient way of synchronizing both scales in this way, is to plot the functional data obtained from experiment on the same graph of our theoretical curves. In this way, we should be able to judge which theoretical curve does our experimental curve map to. We do the comparison differently for intensity and galaxies, i.e, we compare (on the same graph) the experimental curve for z^2I versus redshift with the theoretical curves of the same and similarly the experimental curve for number density $n(z)$ versus redshift with the theoretical curve of the same. It is possible for the experimental curve not to fit any of our theoretical curves but to lie between any two of them. If this is the case, then one can choose a value of $R(t_o)$ between the two values of $R(t_o)$ of our theoretical curves sandwiching the experimental one and use it in the relevant program (depending on whether one is looking at z^2I or $n(z)$)). If the experimental curve cannot fit any of our resulting theoretical curves, then we can again make a new choice of $R(t_o)$ between the two values of $R(t_o)$ of the two theoretical curves that now sandwich the experimental curve. Using this value of $R(t_o)$ in the relevant program, new theoretical curves result and it can easily be seen if the experimental curve fits any of these theoretical

curves. If the experimental curve does not fit any of these resulting theoretical curves, the above process is repeated until right theoretical curve that fits the experimental one is obtained. If such a theoretical curve that fits the experimental curve is found, then the parameter values used in the program like $R(t_o)$, ρ, and κ can be regarded to be the radius of the universe, the density of the universe, and the nature of the universe (whether flat, closed, or open) respectively.

It can be concluded that the hypothesis of the luminous matter being homogeneously distributed in a Friedmann universe is theoretically not in contradiction with the observed data as far as this investigation is concerned. However, the final answer to this question lies in the experimental work done as outlined above.

CHAPTER FIVE

5. SUMMARY, CONCLUSION AND RECOMMENDATION

5.1 SUMMARY AND CONCLUSION

A lot of work has been done and research carried out in an attempt to understand our universe. Unfortunately, none of this work has been able to satisfactorily answer the long disturbing question as to whether or not visible matter is homogeneously distributed in accordance with the Friedmann universe. The problem with this work is due to its dependence on three-dimensional catalogues that rely on methods of inaccurate distance measurements. In an attempt to answer this question and establish the validity of the cosmological principle, we have adopted an approach which does not involve any distance measurements, but which can make use of the data that has become available through these new catalogues. Based on the measurements of the light intensity I, redshift z, we leave our results in a state suitable for comparison with experimental results from data not involving distance measurements. If the experimental curve for data involving no distance measurements cannot fit any of our theoretical curves no matter the choice of parameters that we make, then we rule out that luminous matter is homogeneously distributed in a Friedmann universe. We would consequently have no reason to believe that our universe can be modeled by the Friedmann universe. Subject to the availability of such data, we have laid the basis for satisfactorily solving this puzzling question and establishing the validity of the cosmological principle.

In conclusion however, as far as this investigation is concerned, our universe is indeed Friedmann on large scales.

5.2 RECOMMENDATION

As was seen from the discussion of the results, a number of observations made from our astronomical quantities (luminous matter) are in accordance with the expectations of a Friedmann universe. Nevertheless, further experimental work involving no distance measurements should be done and the results compared with this work for the right conclusion to be drawn.

REFERENCES

[1]. Encrenaz T. and Bibring P.J., The Solar System, springer-Verlag Berlin Heideberg, New York (1995).

[2]. Friesch U., Bec J., Villone B., *Singularities and the distribution of Density in the Burgers/Adhesion Model, arXiv:cond-mat/9912110 (1999).*

[3]. Kutner L. Marc, Astronomy: A physical perspective, John Wiley and sons,inc. (1987).

[4]. Meisner et.al. Gravitation, Bell and Howell company, U.S.A (1973).

[5]. Protheroe et.al, Exploring the Universe, $2^{nd}ed., BellandHowellCompany, London$(1979).

[6]. Shandarin segei F., *Three-dimensional Burgers' Equation as a Model for the Large Scale Structure Formation in the Universe, arXiv:astro-phy/9507082 (1995).*

[7]. Will M. Clifford, Was Einstein Right? $2^{nd}ed., pgs440-467, OxfordUniversityPress, London$(1993).

[8]. Zeilik Michael and Gaustal John, Astronomy: The cosmic perspective, $2^{nd}ed., JohnWileyandsons, inc.NewYork$(1990).

[9]. Zeilik Michael, The Evolving Universe, $6^{th}ed., JohnWileyandsons, inc. NewYork$(1995).

[10]. Wald, Robert M., General Relativity, University of Chicago Press, Ltd., London (1994).

[11]. Berry Michal, Principles of Cosmology and Gravitation, Institute of Physics Publishing (1989).

[12]. Sylos Labini F., Montuori M., Pietronero L., *Scale-invariance of Galaxy Clustering. arXiv:astro-phy/9711073 (1997).*

[13]. Sylos Labini F., and Pietronero L., *Multifractality as a Link Between Luminosity and Space Distribution of Visible matter, arXiv:astro-phy/9605053 (1996).*

[14]. Vergassola M., Dubrulle B., Frisch U., and Noullez A., *Burgers' Equation, Devil's Staircases and the Mass Distribution for Large-scale Structures, Astron. Astrophys.* **289**,*325-356 (1994).*

[15]. Benard J.T., *Observing the Universe, Theoretical Astrophysics Center and Niels Bohr Institute (1993).*

[16]. Bak Per et.al, *Self-Organized Criticality: An Explanation of 1/f Noise, Physical Review Letters, The American Physical Society,* **59**, *No.4 (1987).*

[17]. Eckmann Jean-pierre and Procaccia Itamar, *Multiscaling generated by Time Dependent Classical Field theories, Elsevier Science Publishers, Physics Letters A* **182**, *93-98 (1993).*

[18]. Jones Benard J.T., *The Origin of scaling in the Galaxy Distribution, T.A.C, Copenhagen,* **000**, *000-000 (1994).*

[19]. Kardar Mehran et.al, *Dynamic Scaling of Growing interfaces, Physical Review Letters, The American Physical Society,* **56**, *No.9 (1986).*

[20]. Sylos Labini F., and Pietronero L., *Stochastic Aaggregation Model for the Multifractal Distribution of Matter, arXiv:astroph/9504012 (1995).*

[21]. Sylos Labini F., *Astrophys.J.,* **433**,*464 (1994).*

[22]. Pietronero L., Montuori M., and Sylos Labini F., *The Debate of Galaxy Correlations*

and its Theoretical Implications, arXiv:astro-phy/9510027 (1995).

[23]. Sylos Labini F., *Astrophys.J., Lett.* **L5**,*382, (1992).*

[24]. Hubble E., *Nat. Acad.Sci.Proc.*,**15**,*168 (1929).*

[25]. Durrer Ruth and Eckmann Jean-Pierre, *Angular Projections of Fractal sets, arXiv: astrophy/9702116v2 (1997).*

[26]. Rebeiro Marcelo B., *On Modelling a Relativistic Hierarchical (Fractal) Cosmology by Tolman's Space-time 1, Theory, Astrophys.J.*, **388**,*1-8 (1992).*

[27]. Rebeiro Marcelo B., *On Modelling a Relativistic Hierarchical (Fractal) Cosmology by Tolman's Space-time 2, Analysis of the Einstein-desitter Model, Numerical Results, Astrophys.J.*, **395**:*29-33, (1992).*

[28]. Rebeiro Marcelo B., *On Modelling a Relativistic Hierarchical (Fractal) Cosmology by Tolman's Space-time 3, Analysis of the Einstein-desitter Model, Numerical Results, Astrophys.J.*,**415**,*469-485, (1993).*

[29]. Jastro R. and Malcom H., Astronomy: Fundamentals and Frontiers, pgs 124-126